A Wave Propagation Method for Three-Dimensional Hyperbolic Conservation Laws[1]

Jan Olav Langseth* and Randall J. LeVeque†

*Norwegian Defence Research Establishment, P.O. Box 25, N-2027 Kjeller, Norway; and †Departments
of Mathematics and Applied Mathematics, University of Washington, Seattle, Washington 98195-2420
E-mail: rjl@amath.washington.edu

A class of wave propagation algorithms for three-dimensional conservation laws and other hyperbolic systems is developed. These unsplit finite-volume methods are based on solving one-dimensional Riemann problems at the cell interfaces and applying flux-limiter functions to suppress oscillations arising from second-derivative terms. Waves emanating from the Riemann problem are further split by solving Riemann problems in the transverse directions to model cross-derivative terms. With proper upwinding, a method that is stable for Courant numbers up to 1 can be developed. The stability theory for three-dimensional algorithms is found to be more subtle than in two dimensions and is studied in detail. In particular we find that some methods which are unconditionally unstable when no limiter is applied are (apparently) stabilized by the limiter function and produce good looking results. Several computations using the Euler equations are presented including blast wave and complex shock/vorticity problems. These algorithms are implemented in the CLAWPACK software, which is freely available.   © 2000 Academic Press

Key Words: finite-volume methods; high resolution; wave propagation; three dimensions; Euler equations; software.

1. INTRODUCTION

This paper describes an unsplit method for solving three-dimensional conservation laws, i.e., equations of the form

$$q_t + f(q)_x + g(q)_y + h(q)_z = 0, \tag{1}$$

where $q \in \mathbb{R}^m$ is the conserved quantity. It is well known that these equations may develop shock waves or contain other discontinuities. The existence of regions where the solution changes abruptly places special requirements on the numerical methods to be used. Traditionally, simple numerical schemes suffer from dissipative and dispersive effects, resulting in inappropriate representation of these discontinuities. This is reflected in the solution as spurious oscillations or excessive smearing in the vicinity of the discontinuity. Since the occurrence of discontinuous waves is a significant feature of hyperbolic problems, much effort has been made to construct robust methods producing sharp and monotone representations.

One special initial value problem is of major importance, both in its own and in the development of efficient numerical methods. This is the Riemann problem which consists of the equation $q_t + f(q)_x = 0$ together with the initial condition

$$q(x, 0) = \begin{cases} q_l & x < 0 \\ q_r & x \geq 0, \end{cases} \tag{2}$$

where q_l and q_r are constants. With certain assumptions on the flux function f, it is always possible, in principle, to solve the Riemann problem if the states q_l and q_r are sufficiently "close"; see [22, 39]. The solution consists of waves traveling with finite velocities. These waves may either be discontinuous waves like shock waves or smooth rarefaction waves. The similarity solution of this initial-value problem depends on the ratio x/t. Due to this simplification, it is possible to solve any scalar problem. Also for many important nonlinear systems, the Riemann problem can be solved, e.g., the Euler equations of gas dynamics [16, 39]. The procedure for constructing the solution of a Riemann problem will be called a Riemann solver.

The history of the development of numerical methods for hyperbolic conservation laws is long and rich. The wave propagation method described in this paper falls into the tradition of methods based on solving Riemann problems, which originated with the work of Godunov [15]. For a general overview of such methods and many references, see, for example, [14, 18, 25, 44].

A common approach to solving multidimensional hyperbolic problems is to apply dimensional splitting; see [9, 41]. The idea is to iterate on one-dimensional problems. The popularity of these algorithms is due to their simplicity and the fact that they produce surprisingly good results. Any one-dimensional scheme is easily extended to the multidimensional case using this approach. However, it is well known that dimensional splitting has several disadvantages. Since the strategy only involves flow in the coordinate directions, the solution may be affected by the grid orientation. The implementation of boundary conditions and adaptive refinement may also be complicated using this strategy.

In unsplit methods, information is propagated in a multidimensional way. The unsplit scheme to be presented was first described in an unfinished form in [19] and later in a state close to the present in the thesis of the first author [21]. One-dimensional Riemann problems are solved at the interfaces. Limiter functions are applied to suppress spurious oscillations arising from second-derivative terms. The left-going and right-going waves are split into parts propagating in the transverse direction by solving Riemann problems in coordinate directions tangential to the interfaces. This models cross-derivative terms necessary for obtaining both a stable and a formally second-order scheme. The scheme extends the approach used for two space dimensions [26, 28] and the advection scheme for three-dimensional

problems considered in [27]. The 3D wave propagation scheme is implemented in Fortran and is included in the software package CLAWPACK (Conservation LAW PACKage) [29]. This package includes routines for solving a wide range of hyperbolic problems and contains a selection of different Riemann solvers, boundary conditions, etc. CLAWPACK is freely available on the Web [29].

This method is similar in spirit to other multidimensional methods using one-dimensional Riemann problems at the cell interfaces; see [2, 5, 7, 24, 31, 34, 37, 38, 45]. However, an algorithmic difference is that the Riemann problem is based on the solution values at the beginning of the time step, and that cross-derivative terms are implemented due to the transverse propagation of the emanating waves. In other methods, such as that of Colella [7], the states involved in the Riemann problem are based on an interpolation in which the transverse terms based on characteristic decompositions in the transverse directions are included before the Riemann problem is solved. A disadvantage to most of these multidimensional approaches (including ours) is that a large number of Riemann problems (or characteristic decompositions) must generally be solved in each grid cell in each time step. For our algorithms the exact number depends on how many transverse terms are included, as described in Section 2.5. For nonlinear problems most of these Riemann solutions are simpler and cheaper than the basic Riemann solver applied normal to each grid edge, as discussed in that section.

We should note that for many problems dimensional splitting can be used successfully. This requires only solving the normal Riemann problem and applying strictly one-dimensional high-resolution methods. The cross-derivative terms are modeled automatically by the fractional step nature of the algorithm. Dimensional splitting is one of the options provided in CLAWPACK and typically runs about twice as fast as the full multidimensional algorithm described here on the Euler equations. Conversely, however, the methods described here require only about twice as much time on a given grid and do yield better results in some situations. Since in three space dimensions refining the grid by a factor of 2 requires 16 times as much work, there are definite advantages to using the best possible algorithm on a given grid, even if the cost is slightly higher.

In the wave propagation algorithm, it is not necessary to evaluate the flux functions explicitly. As a consequence, the algorithm may as well be applied on systems in non-conservative form. In CLAWPACK, the scheme is implemented so that it is applicable to quasilinear problems having the form

$$\kappa(x, y, z)q_t + A(q, x, y, z, t)q_x + B(q, x, y, z, t)q_y + C(q, x, y, z, t)q_z$$
$$= \Psi(q, \kappa, x, y, z, t). \tag{3}$$

Recent work on acoustic and elastic waves in heterogeneous media [11, 13] shows that these methods can be extremely useful even for linear problems since the solution of the Riemann problem accurately models the transmission and reflection of waves at a material interface. The three-dimensional algorithm developed here should be applicable to problems of this type as well. In this paper, we focus on the conservation law (2) and refer to [28] for a discussion of how to apply CLAWPACK routines to this more general class of problems. In Section 2, the wave propagation scheme is derived. In the process of deriving this scheme, the one-dimensional and two-dimensional versions are briefly reviewed. In Section 3, numerical results are given for three test problems involving the Euler equations: a radially symmetric smooth solution where second-order accuracy can be verified, an initially spherical shock

wave expanding in a slab between two parallel walls, and finally a fully 3D problem in which shock waves are used to produce vorticity.

Stability is the topic of Section 4. A von Neumann approach is used to shed some light on the question of stability for the wave propagation scheme and how the use of limiters affects this property. With proper upwinding, a method that is stable for Courant numbers up to 1 can be developed. However, the stability theory for three-dimensional algorithms is found to be more subtle than that for two dimensions and we study this in detail. In particular, we find that some methods which are unconditionally unstable when no limiter is applied are (apparently) stabilized by the limiter function and produce good looking results.

2. WAVE PROPAGATION ALGORITHMS

In this section we will derive the three-dimensional wave propagation scheme. This will generalize the schemes for two-dimensional systems described in [28] and scalar three-dimensional problems from [27]. We give a brief review of the one-dimensional wave propagation method, but in order to avoid substantial repetition we assume that the reader is familiar with the multidimensional notation and the ideas of [27, 28].

We assume that the three-dimensional system of conservation laws (1) is hyperbolic, i.e., that the matrix $\alpha f'(q) + \beta g'(q) + \gamma h'(q)$ has real eigenvalues and a complete set of eigenvectors for any real α, β, and γ with $|\alpha| + |\beta| + |\gamma| > 0$. Define a regular grid with constant spacing $\Delta x, \Delta y$, and Δz. Let C_{ijk} denote the cell $[x_i, x_{i+1}] \times [y_j, y_{j+1}] \times [z_k, z_{k+1}]$, where $x_i = i\Delta x$, etc. Likewise let Δt denote the time step, and let $t_n = n\Delta t$ the time levels.

To derive the numerical scheme we primarily consider two linear problems, namely the scalar equation

$$q_t + uq_x + vq_y + wq_z = 0 \tag{4}$$

and the linear system

$$q_t + Aq_x + Bq_y + Cq_z = 0. \tag{5}$$

The essential ideas and difficulties in three-dimensional wave propagation appear already with these linear problems. The extension to nonlinear systems is then immediate following the approach used already in two space dimensions in [28]. Unless otherwise noted, we will often assume that the advection velocities are positive as a specific example.

The wave propagation schemes will be written in the same form as in that paper,

$$\bar{Q}_{ijk} = Q_{ijk} + \Delta_{ijk}^{up} - \frac{\Delta t}{\Delta x}(\tilde{F}_{i+1,jk} - \tilde{F}_{ijk}) - \frac{\Delta t}{\Delta y}(\tilde{G}_{i,j+1,k} - \tilde{G}_{ijk})$$

$$- \frac{\Delta t}{\Delta z}(\tilde{H}_{ij,k+1} - \tilde{H}_{ijk}), \tag{6}$$

where $\bar{Q}$ represents the numerical solution at the time step t_{n+1}. The term Δ_{ijk}^{up} includes the donor-cell part, i.e., a (one-dimensional) first-order upwind scheme applied coordinate-wise. The $\tilde{F}, \tilde{G}$, and $\tilde{H}$ terms take care of the approximations of the higher order derivatives, including cross-derivative terms. The flux functions will not be needed explicitly, and as a consequence, the scheme can easily be applied to a wider range of hyperbolic problems.

2.1. Schemes for Linear 1D Problems

Essential features of the wave propagation schemes are the so-called increment and correction waves. The former refers to the constant state waves given from the solution of the (approximate) Riemann problem, while the correction waves are piecewise linear waves used for obtaining second-order accuracy. These features are best illustrated by using the simple scalar advection equation

$$q_t + u q_x = 0, \quad u > 0. \tag{7}$$

The conservative scheme for one-dimensional problems reads

$$\bar{Q}_i = Q_i - \frac{\Delta t}{\Delta x}(F_{i+1} - F_i), \tag{8}$$

where the numerical flux F_i approximates the exact flux; i.e.,

$$F_i \approx \frac{1}{\Delta t} \int_{t_n}^{t_{n+1}} f(q(x_i, \cdot)) \, dt.$$

As in standard second-order Godunov methods [25, 48], assume that the solution at time t_n is piecewise linear. The solution at time t_{n+1} is obtained by simply shifting the profile a distance $u\Delta t$. The situation close to the interface x_i then looks as depicted in Fig. 1. Since the problem is linear, the wave entering cell C_i may be split into a piecewise constant and a piecewise linear wave. These waves are named increment and correction waves, respectively. It is easily seen that the numerical flux in this case reads

$$F_i = u Q_{i-1} + \frac{1}{2}u\left(1 - u\frac{\Delta t}{\Delta x}\right)\Delta x \sigma_{i-1}, \tag{9}$$

where σ_{i-1} denotes the slope of the solution in cell C_{i-1}. The first term at the right-hand side of (9) corresponds to the flux contribution from the increment wave, while the last term is the contribution from the correction wave. Note that the increment wave alone yields the first-order upwind scheme and that the correction wave may correct this into a second-order scheme if the slope is chosen correctly.

Next, consider the linear system $f(q) = Aq$, where A is a constant $m \times m$ matrix with eigenvalues λ^p and eigenvectors r^p. Since A has a complete set of eigenvectors, the matrix
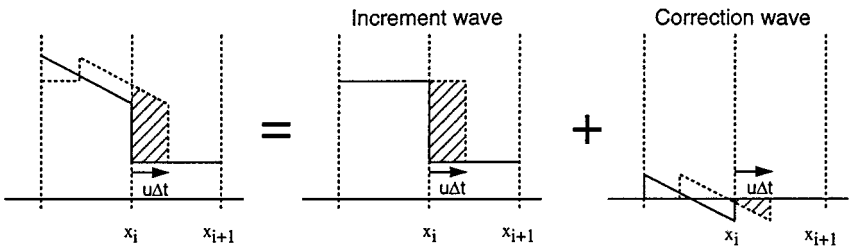
FIG. 1. The piecewise linear function can be split into a constant state wave (the increment wave) and a piecewise linear wave with integral zero (the correction wave).

is diagonalizable; i.e.,

$$A = R\Lambda R^{-1},$$

where $R = [r^1|r^2|\ldots|r^m]$ is the eigenvector matrix and $\Lambda = \text{diag}(\lambda^1, \lambda^2, \ldots, \lambda^m)$. For $a \in \mathbb{R}$ let

$$a^+ = \max(0, a), \quad a^- = \min(0, a).$$

Define the positive and negative parts of A as

$$A^+ = R\Lambda^+ R^{-1}, \quad A^- = R\Lambda^- R^{-1}, \tag{10}$$

where $\Lambda^\pm = \text{diag}(\lambda^{1\pm}, \lambda^{2\pm}, \ldots, \lambda^{m\pm})$.

The solution of the Riemann problem defined by Q_{i-1} and Q_i consists of m discontinuities moving with velocities λ^p. Each jump is a scalar multiple of the eigenvector; i.e., $\mathcal{W}_i^p = \alpha_i^p r^p$. Hence, the jump $\Delta Q_i = Q_i - Q_{i-1}$ may be written as

$$\Delta Q_i = \sum_p \mathcal{W}_i^p.$$

The first-order Godunov flux is defined as

$$F_i^G = f\left(Q_i^0\right),$$

where Q_i^0 denotes the solution at $x/t = 0$ of the Riemann problem with left state Q_{i-1} and right state Q_i. For the linear system this intermediate state equals

$$Q_i^0 = Q_{i-1} + \sum_{\lambda^p<0} \mathcal{W}_i^p = Q_i - \sum_{\lambda^p>0} \mathcal{W}_i^p.$$

Hence, the Godunov flux reads

$$F_i^G = AQ_{i-1} + A^- \Delta Q_i = AQ_i - A^+ \Delta Q_i.$$

For the numerical scheme (8) we get

$$\bar{Q}_i = Q_i - \frac{\Delta t}{\Delta x}(A^+ \Delta Q_i + A^- \Delta Q_{i+1}). \tag{11}$$

The expression $A^+ \Delta Q_i = \sum_p (\lambda^p)^+ \mathcal{W}_i^p$ gives the flux contribution from the waves entering cell C_i from the Riemann problem at the left interface, while $A^- \Delta Q_{i+1}$ gives the flux from the waves entering the same cell from the Riemann problem at the right interface. These piecewise constant waves, emanating from the Riemann problems, will be named increment waves, as a generalization of similar waves in the scalar case.

2.2. Second-Order Corrections

The scheme considered above is first-order accurate only. To increase the order, (8) is rewritten as

$$\bar{Q}_i = Q_i + \Delta_i^{up} - \frac{\Delta t}{\Delta x}(\tilde{F}_{i+1} - \tilde{F}_i), \tag{12}$$

where Δ_i^{up} equals the upwind increment (the effect of the Godunov fluxes) obtained from (11); i.e.,

$$\Delta_i^{up} = -\frac{\Delta t}{\Delta x}(A^+\Delta Q_i + A^-\Delta Q_{i+1}). \tag{13}$$

The term $\tilde{F}_i$ is used to update the solution so that second-order accuracy is achieved. This is based on the Lax–Wendroff scheme, though in Section 4 we will discuss the possible merits of using other second-order schemes as the starting point.

The flux for the Lax–Wendroff scheme may be written as

$$F_i = F_i^G + \frac{1}{2}|A|\left(1 - \frac{\Delta t}{\Delta x}|A|\right)\Delta Q_i,$$

where $|A| = A^+ - A^-$. Hence, a natural choice for $\tilde{F}_i$ is

$$\tilde{F}_i = \frac{1}{2}|A|\left(1 - \frac{\Delta t}{\Delta x}|A|\right)\Delta Q_i$$
$$= \frac{1}{2}\sum_p |\lambda^p|\left(1 - \frac{\Delta t}{\Delta x}|\lambda^p|\right)\mathcal{W}_i^p. \tag{14}$$

The Godunov scheme exhibits strong numerical dissipation and discontinuities in the solution are smeared, causing low accuracy. The Lax–Wendroff scheme, on the other hand, is more accurate in smooth parts of the solution. But near discontinuities, numerical dispersion generates oscillations, also reducing the accuracy.

A successful approach to suppressing these oscillations is to apply flux limiting. This is obtained by replacing the wave $\mathcal{W}_i^p = \alpha_i^p r^p$ by

$$\tilde{\mathcal{W}}_i^p = \Phi(\theta_i^p)\mathcal{W}_i^p, \tag{15}$$

where θ_i^p measures the smoothness of the solution. A standard way of doing this is to consider the ratio of wave strengths α_i^p in the upwind direction; i.e.,

$$\theta_i^p = \begin{cases} \alpha_{i-1}^p/\alpha_i^p, & \lambda^p > 0 \\ \alpha_{i+1}^p/\alpha_i^p, & \lambda^p < 0. \end{cases} \tag{16}$$

The limiters used here are originally constructed to ensure both second-order accuracy and TVD properties for scalar conservation laws. For a detailed discussion of such methods, see [14, 25, 43, 44]. The TVD concept is not applicable in the system case directly, but applying this strategy to the characteristic equations, as done implicitly here, produces steep and monotone approximations of discontinuities.

Note that $\Phi = 1$ yields the Lax–Wendroff scheme, while $\Phi = 0$ yields the Godunov scheme. In Section 4.3 we also study the Fromm scheme and the Beam–Warming scheme, both being second-order accurate. Here we simply note that $\Phi = \theta$ gives the latter scheme, while $\Phi = (1 + \theta)/2$ gives the former. Some common limiters are

$$\text{minmod:} \quad \Phi(\theta) = \max(0, \min(1, \theta))$$
$$\text{superbee:} \quad \Phi(\theta) = \max(0, \min(1, 2\theta), \min(2, \theta))$$
$$\text{monotonized centered (MC):} \quad \Phi(\theta) = \max(0, \min((1 + \theta)/2, 2, 2\theta)).$$

Minmod is the most diffusive limiter of the above, in the sense that it adds less downwind contribution. This limiter selects the wave with the smallest norm of the two compared, provided the jumps across the waves are in the same direction; i.e., the wave strengths have a common sign. If not, the wave is entirely suppressed. On the other hand, the superbee limiter is known to be "overcompressive"; i.e., it tends to sharpen profiles into discontinuities. The MC limiter seems to be a good choice in most situations.

As a generalization of the correction waves in the scalar case, the piecewise linear waves used in the second-order update will also be referred to as correction waves.

2.3. The Propagation of the Increment Wave in Three Dimensions

The one-dimensional algorithm summarized above can be viewed as a two-step procedure. The increment waves are used to define the donor-cell upwind term Δ_i^{up} in (12), and then correction waves (based on the piecewise linear reconstruction) are used to define fluxes $\tilde{F}_i$. In two and three dimensions the increment waves should also be propagated in the transverse direction(s) to improve accuracy and stability. The correction waves might also be transversely propagated. For the two-dimensional case, the wave propagation algorithms with transverse terms have been presented in detail in [27, 28]. Here we concentrate on describing the extensions to three dimensions, assuming familiarity with those papers and using the same basic approach and notation. The donor-cell update is denoted by Δ_{ijk}^{up} and the fluxes resulting from all correction terms are denoted by $\tilde{F}_{ijk}$, $\tilde{G}_{ijk}$, and $\tilde{H}_{ijk}$. These corrections include both the second-order correction waves and the effects of any transverse propagation of increment or correction waves. Cell averages are updated based on all of these values using formula (6).

In the three-dimensional case we still only solve one-dimensional Riemann problems. The increment and correction waves in 3D are simple extensions of those obtained in one dimension. A Riemann problem is first solved normal to each cell interface and then this Riemann solution is decomposed in the transverse directions by solving a set of simplified "transverse Riemann problems."

In each time step we begin by initializing Δ_{ijk}^{up} and the correction fluxes to zero:

$$\Delta_{ijk}^{up} = \tilde{F}_{ijk} = \tilde{G}_{ijk} = \tilde{H}_{ijk} = 0. \tag{17}$$

These are then repetitively updated based on the solutions to various Riemann problems at cell interfaces nearby. Rather than presenting the formula for one particular flux such as $\tilde{F}_{ijk}$ in terms of all the data nearby, it is much clearer and more concise to describe the manner in which the solution to each Riemann problem is used in updating nearby fluxes. This is

also how the algorithms are implemented in the CLAWPACK code, and complete details may be found by examining the software.

The description below will focus primarily on the solution of the Riemann problem defined at the interface x_i between cells $C(i-1, jk)$ and $C(ijk)$. We describe how the resulting waves update the upwind terms $\Delta_{i-1,jk}^{up}$ and Δ_{ijk}^{up}, the correction flux $\tilde{F}_{ijk}$ at this interface, and nearby $\tilde{G}$ and $\tilde{H}$ fluxes. An analogous procedure is followed at each interface in the y direction and in the z direction.

Propagating the waves in different ways transverse to the interface leads to a family of possible methods with different accuracy and stability properties. These will be built up over the next several sections. Stability analysis is presented in Section 4.

2.3.1. Scalar Advection

For the scalar equation (4), the simple first-order donor-cell upwind scheme results from simply setting

$$\Delta_{ijk}^{up} := \Delta_{ijk}^{up} - \frac{\Delta t}{\Delta x} u^+ (Q_{ijk} - Q_{i-1,jk})$$

$$\Delta_{i-1,jk}^{up} := \Delta_{i-1,jk}^{up} - \frac{\Delta t}{\Delta x} u^- (Q_{ijk} - Q_{i-1,jk})$$

and leaving all correction fluxes equal to zero. The Riemann solution consists of a single wave $\Delta_x Q_{ijk} = Q_{ijk} - Q_{i-1,jk}$ which propagates to the right or left depending on the sign of u. This results in the upwind term

$$\Delta_{ijk}^{up} = -\frac{\Delta t}{\Delta x} (u^+ \Delta_x Q_{ijk} - u^- \Delta_x Q_{i+1,jk}) - \frac{\Delta t}{\Delta y} (v^+ \Delta_x Q_{ijk} - v^- \Delta_x Q_{i,j+1,k})$$

$$- \frac{\Delta t}{\Delta z} (w^+ \Delta_x Q_{ijk} - w^- \Delta_x Q_{ij,k+1})$$

after all Riemann problems are solved in each direction. The stability condition of this scheme is easily seen to be $|u|\frac{\Delta t}{\Delta x} + |v|\frac{\Delta t}{\Delta y} + |w|\frac{\Delta t}{\Delta z} \leq 1$ (see Section 4). To increase both stability and accuracy, the increment wave is advected in the direction of the velocity vector (u, v, w) (Fig. 2). This yields the "shift and average" scheme [27], in which the piecewise constant function defined by the cell values Q_{ijk} is shifted according to the velocity and then averaged back onto the grid. This method is clearly stable for Courant numbers up to 1.

This shift and average scheme is defined using the same term Δ_{ijk}^{up} as above, but now the nearby $\tilde{G}$ and $\tilde{H}$ fluxes are updated to capture the portion of the wave which should be transferred into neighboring cells. Suppose, for example, that the velocities, u, v, and w are all positive, and consider the update to $\tilde{G}_{i,j+1,k}$ given by the increment wave originating from the interface $x = x_i$. (The wave is defined by the jump $-\Delta_x Q_{ijk} = Q_{i-1,j,k} - Q_{ijk}$ and the velocity vector.)

$$\tilde{G}_{i,j+1,k} := \tilde{G}_{i,j+1,k} - \frac{1}{\Delta t} \frac{1}{\Delta z} \frac{1}{\Delta x} \int_{t_n}^{t_{n+1}} \int_{z_k+w(t-t_n)}^{z_{k+1}} \int_{x_i}^{x_i+u(t-t_n)} v \Delta_x Q_{ijk} \, dx \, dz \, dt,$$

$$= \tilde{G}_{i,j+1,k} - \frac{1}{2} \frac{\Delta t}{\Delta x} u v \Delta_x Q_{ijk} + \frac{1}{3} u v w \frac{\Delta t}{\Delta x} \frac{\Delta t}{\Delta z} \Delta_x Q_{ijk}. \quad (18)$$
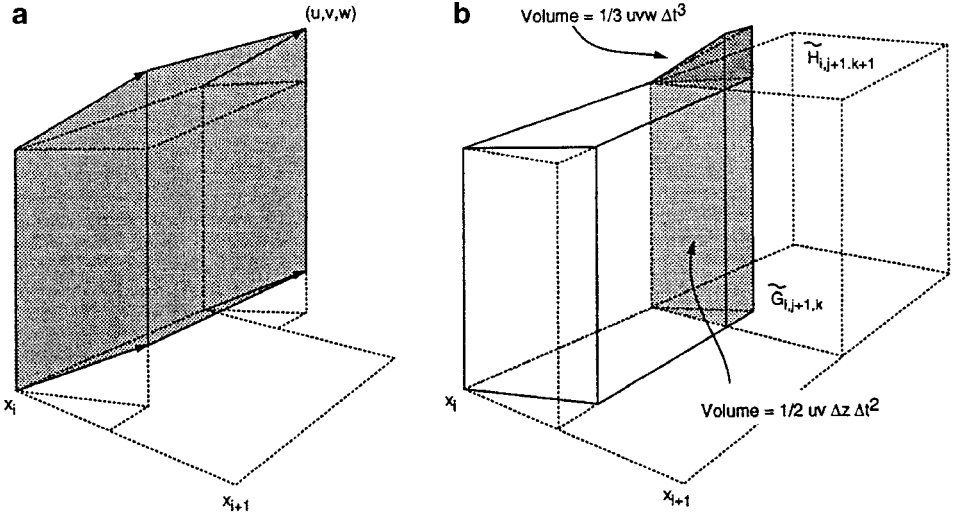
FIG. 2. (a) The volume covered by the increment wave, when the velocities are positive. (b) The volume used in updating the cells $C_{ij,k+1}$ and $C_{i,j+1,k+1}$.

Another way of deriving this expression is to consider the volume in cell $C_{i,j+1,k}$ covered by the wave, which equals $\frac{1}{2}uv\Delta t^2\Delta z - \frac{1}{3}uvw\Delta t^3$. Since the wave carries the constant jump $-\Delta_x Q_{ij}$, the appropriate flux update equals (18). Likewise, the volumes covered by this wave in the other neighboring cells are

$$C_{ij,k+1}: \quad \frac{1}{2}uv\Delta t^2\Delta z - \frac{1}{3}uvw\Delta t^3$$

$$C_{i,j+1,k+1}: \quad \frac{1}{3}uvw\Delta t^3.$$

These volumes are shown in Fig. 2b. The actual change in the solution equals these volumes times the jump $-\Delta_x Q_{ijk}$ and is obtained by updating the fluxes. There are several ways of distributing the solution updates between the fluxes in the scalar case. Here, an approach different from that in [27] will be used, since this will be in agreement with the appropriate terms in the system case.

When the velocities are positive, the flux updates are

$$\tilde{G}_{i,j+1,k} := \tilde{G}_{i,j+1,k} - \frac{1}{2}uv\frac{\Delta t}{\Delta x}\Delta_x Q_{ijk} + \frac{1}{6}uvw\frac{\Delta t}{\Delta x}\frac{\Delta t}{\Delta z}\Delta_x Q_{ijk}$$

$$\tilde{G}_{i,j+1,k+1} := \tilde{G}_{i,j+1,k+1} - \frac{1}{6}uvw\frac{\Delta t}{\Delta x}\frac{\Delta t}{\Delta z}\Delta_x Q_{ijk}$$

$$\tilde{H}_{ij,k+1} := \tilde{H}_{ij,k+1} - \frac{1}{2}uv\frac{\Delta t}{\Delta x}\Delta_x Q_{ijk} + \frac{1}{6}uvw\frac{\Delta t}{\Delta x}\frac{\Delta t}{\Delta y}\Delta_x Q_{ijk}$$

$$\tilde{H}_{i,j+1,k+1} := \tilde{H}_{i,j+1,k+1} - \frac{1}{6}uvw\frac{\Delta t}{\Delta x}\frac{\Delta t}{\Delta y}\Delta_x Q_{ijk}.$$

$$(19)$$

Doing the same for increment waves originating from interfaces in y and z gives a scheme identical to the shift and average scheme. Hence, we have obtained a first-order scheme

with the desired stability limit, i.e., stability for Courant numbers less than or equal to 1, as described further in Section 4.

Note that the update of $\tilde{G}_{i,j+1,k}$ consists of two terms. The first term, also found in the two-dimensional wave propagation schemes (cf. [28]) corresponds to the part of the wave moving into cells sharing an interface with either of the cells defining the Riemann problem, i.e., $C_{i-1,jk}$ and C_{ijk}. This feature will be named *transverse propagation*. The last update, named *double transverse propagation*, is a pure three-dimensional contribution and is caused by the part of the wave moving into cells only sharing an edge with one of these cells.

Also note that the updates of $\tilde{G}$ and $\tilde{H}$ above contain a difference in x. Hence, these updates will account for terms like $\frac{1}{2}uvq_{xy}$ and $\frac{1}{6}uvwq_{xyz}$ in a Taylor expansion. This will be studied to some detail in the next section.

2.3.2. Linear Systems

Here we consider the propagation of the increment waves for the linear system (5). Since the problem is assumed to be hyperbolic, A, B, and C are diagonalizable. We define the positive and negative parts of B similar to what was done for A in (10); i.e.,

$$B^{\pm} = W M^{\pm} W^{-1}, \tag{20}$$

where W is the eigenvector matrix, and M the diagonal eigenvalue matrix. The eigenvalues are μ^q, and the associated eigenvectors w^q. Likewise, let ν^l and s^l denote the eigenvalues and eigenvectors of C. Then we define

$$C^{\pm} = S N^{\pm} S^{-1},$$

where S is the eigenvector matrix and N the diagonal matrix with the eigenvalues ν^l as entries.

Before proceeding with the three-dimensional propagation of the increment wave, we expand $q(x, y, z, t + \Delta t)$ in a Taylor series including terms up to third order in Δt. This is useful for understanding how the specific wave propagation affects the solution. Due to the large number of terms, we only consider those differentiated first in x.

The flux updates resulting from a single interface in x should lead to approximations of these terms, which are

$$\Delta t A q_x + \frac{1}{2}\Delta t^2 (A^2 q_{xx} + BAq_{xy} + CAq_{xz}) - \frac{1}{6}\Delta t^3 (A^3 q_{xxx} + ABAq_{xyz} + ACAq_{xzx}$$

$$+ BA^2 q_{xxy} + B^2 Aq_{xyy} + BCAq_{xzy} + CA^2 q_{xxz} + CBAq_{xyz} + C^2 Aq_{xzz}). \tag{21}$$

The (full) wave propagation scheme to be derived will cover all these terms, except for the $A^3 q_{xxx}$ term. In addition, some fourth-order terms will be accounted for. This is necessary for stability, as discussed in Section 4.

Unless the matrices have a common set of eigenvectors it is not possible to decompose (5) into a system of m scalar advection equations. Nevertheless, it is useful to talk about wave propagation locally even in the general case.

The first step in the algorithm is to solve the one-dimensional Riemann problem normal to the interface, i.e., find (increment) waves $\mathcal{W}_{ijk}^p$ so that $Q_{ijk} - Q_{i-1,jk} = \sum_p \mathcal{W}_{ijk}^p$. This

is exactly the same approach as used in the one-dimensional case. For example,

$$A^-\Delta_x Q_{ijk} = \sum (\lambda^p)^- \mathcal{W}_{ijk}^p, \quad A^+\Delta_x Q_{ijk} = \sum (\lambda^p)^+ \mathcal{W}_{ijk}^p, \tag{22}$$

and

$$\Delta_{ijk}^{up} := \Delta_{ijk}^{up} - \frac{\Delta t}{\Delta x}(A^-\Delta_x Q_{i+1,jk} + A^+\Delta_x Q_{ijk}).$$

Doing the same in the y and z directions yields a scheme in which waves only propagate normal to the cell interfaces, i.e., the donor-cell approach.

Next, every increment wave from the Riemann problem in x is split into waves moving in the y direction; i.e.,

$$\mathcal{W}_{ijk}^p = \sum_q \beta_{ijk}^{pq} w^q. \tag{23}$$

Each $\mathcal{W}_{ijk}^p$ will then update any of the surrounding $\tilde{G}$ fluxes depending on the sign of λ^p. For example, if λ^p and μ^q are both positive, then

$$\tilde{G}_{i,j+1,k} := \tilde{G}_{i,j+1,k} - \frac{1}{2}\frac{\Delta t}{\Delta x}\lambda^p \mu^q \beta_{ijk}^{pq} w^q,$$

similar to the first term in the update in (18). The sum of all contributions to this flux gives

$$\tilde{G}_{i,j+1,k} := \tilde{G}_{i,j+1,k} - \frac{1}{2}\frac{\Delta t}{\Delta x}\sum_q \sum_p (\lambda^p)^+ (\mu^q)^+ \beta_{ijk}^{pqk} w^q. \tag{24}$$

It is easily seen that this is equal to

$$\tilde{G}_{i,j+1,k} := \tilde{G}_{i,j+1,k} - \frac{1}{2}\frac{\Delta t}{\Delta x}B^+ A^+\Delta_x Q_{ijk}. \tag{25}$$

The proper updates for the rest of the $\tilde{G}$-fluxes are

$$\tilde{G}_{i-1,j,k} := \tilde{G}_{i-1,j,k} - \frac{1}{2}\frac{\Delta t}{\Delta x}B^- A^-\Delta_x Q_{ijk}$$

$$\tilde{G}_{ijk} := \tilde{G}_{ijk} - \frac{1}{2}\frac{\Delta t}{\Delta x}B^- A^+\Delta_x Q_{ijk} \tag{26}$$

$$\tilde{G}_{i-1,j+1,k} := \tilde{G}_{i-1,j+1,k} - \frac{1}{2}\frac{\Delta t}{\Delta x}B^+ A^-\Delta_x Q_{ijk}.$$

Exactly the same terms are found in the two-dimensional scheme described in [28].

Note that since

$$B^+ A^+ + B^- A^+ + B^+ A^- + B^- A^- = BA, \tag{27}$$

the flux updates above will result in an approximation to the $\frac{1}{2}\Delta t^2 BAq_{xy}$ term in the Taylor expansion.

Next, consider transverse propagation of the increment wave in the z direction. This results in an update of the $\tilde{H}$ fluxes similar to (25) and (26),

$$
\begin{aligned}
\tilde{H}_{i-1,jk} &:= \tilde{H}_{i-1,jk} - \frac{1}{2}\frac{\Delta t}{\Delta x}C^- A^- \Delta_x Q_{ijk} \\
\tilde{H}_{ijk} &:= \tilde{H}_{ijk} - \frac{1}{2}\frac{\Delta t}{\Delta x}C^- A^+ \Delta_x Q_{ijk} \\
\tilde{H}_{ij,k+1} &:= \tilde{H}_{ij,k+1} - \frac{1}{2}\frac{\Delta t}{\Delta x}C^+ A^+ \Delta_x Q_{ijk} \\
\tilde{H}_{i-1,j,k+1} &:= \tilde{H}_{i-1,j,k+1} - \frac{1}{2}\frac{\Delta t}{\Delta x}C^+ A^- \Delta_x Q_{ijk},
\end{aligned}
\tag{28}
$$

which accounts for $\frac{1}{2}\Delta t^2 C A q_{xz}$ in the Taylor series.

In an implementation, updates like (24) would require the solution of m Riemann problems, in addition to the one necessary for obtaining $\mathcal{W}^p$. In general, this involves too much work. It is also in general too expensive to derive the $A^\pm$ and $B^\pm$ matrices explicitly and then perform matrix–vector multiplications. Instead the left-going flux difference $A^- \Delta_x Q_{ijk}$ and the right-going flux difference $A^+ \Delta_x Q_{ijk}$ are split into eigenvectors w^q of B, yielding transverse-moving waves. This *transverse flux difference splitting* is obtained by solving the following equations for δ_{ijk}^q:

$$
A^- \Delta_x Q_{ijk} = \sum_q \left(\delta_{ijk}^q\right)^- w^q, \quad A^+ \Delta_x Q_{ijk} = \sum_q \left(\delta_{ijk}^q\right)^+ w^q.
\tag{29}
$$

The computations of the flux updates in (25) and (26) are significantly simplified, for example,

$$
B^+ A^+ \Delta_x Q_{ijk} = \sum_q (\mu^q)^+ \left(\delta_{ijk}^q\right)^+ w^q,
\tag{30}
$$

with similar expressions for the rest of the updates. (The number of Riemann problems per interface is now 5, regardless of the size of the system.)

Comparing with (19), the updates caused by the increment waves do not, so far, account for full three-dimensional propagation. To do this, the waves should also move into cells only sharing an edge with the cells defining the Riemann problem, i.e., double transverse propagation. This yields approximations of cross-derivatives like $\frac{1}{6}\Delta t^3 C B A q_{xyz}$. For this term, the proper updates can be shown to be

$$
\begin{aligned}
\tilde{H}_{ij,k+1} &:= \tilde{H}_{ij,k+1} + \frac{1}{6}\frac{\Delta t}{\Delta x}\frac{\Delta t}{\Delta y}C^+ |B| A^+ \Delta_x Q_{ijk} \\
\tilde{H}_{ijk} &:= \tilde{H}_{ijk} + \frac{1}{6}\frac{\Delta t}{\Delta x}\frac{\Delta t}{\Delta y}C^- |B| A^+ \Delta_x Q_{ijk} \\
\tilde{H}_{i,j+1,k+1} &:= \tilde{H}_{i,j+1,k+1} - \frac{1}{6}\frac{\Delta t}{\Delta x}\frac{\Delta t}{\Delta y}C^+ B^+ A^+ \Delta_x Q_{ijk} \\
\tilde{H}_{i,j+1,k} &:= \tilde{H}_{i,j+1,k} - \frac{1}{6}\frac{\Delta t}{\Delta x}\frac{\Delta t}{\Delta y}C^- B^+ A^+ \Delta_x Q_{ijk}
\end{aligned}
\tag{31}
$$

$$\tilde{H}_{i,j-1,k+1} := \tilde{H}_{i,j-1,k+1} + \frac{1}{6}\frac{\Delta t}{\Delta x}\frac{\Delta t}{\Delta y}C^{+}B^{-}A^{+}\Delta_{x}Q_{ijk}$$

$$\tilde{H}_{i,j-1,k} := \tilde{H}_{i,j-1,k} + \frac{1}{6}\frac{\Delta t}{\Delta x}\frac{\Delta t}{\Delta y}C^{-}B^{-}A^{+}\Delta_{x}Q_{ijk}.$$

Six additional updates are also required. These are obtained by replacing i with $i-1$ in the fluxes above and replacing $A^{+}\Delta_{x}Q_{ijk}$ with $A^{-}\Delta_{x}Q_{ijk}$. Note that the updates in (28) and (31) generalize the changes in $\tilde{H}$ in (19). To approximate $BCAq_{xzy}$, similar updates are made to the $\tilde{G}$ fluxes.

The $C^{+}B^{+}A^{+}\Delta_{x}Q_{ijk}$ term in (31) may be interpreted as follows. Each wave $\mathcal{W}_{ijk}^{p}$ in the expansion of $\Delta_{x}Q_{ijk}$ is split into waves moving in the y direction as in (23). Then each $\beta^{pq}w^{p}$ is split into waves moving in the z direction; i.e., $\beta^{pq}w^{q} = \sum_{l}\gamma^{pql}s^{l}$. It is easily seen that

$$C^{+}B^{+}A^{+}\Delta_{x}Q_{ijk} = \sum_{l}\sum_{q}\sum_{p}(\lambda^{p})^{+}(\mu^{q})^{+}(\nu^{l})^{+}\gamma^{pql}s^{l}. \tag{32}$$

Regarding the implementation of these terms we do the same as done in (29) and (30).

The flux differences $A^{\pm}\Delta_{x}Q_{ijk}$ are split in the y direction accordingly. This yields the transverse wave strengths $(\delta^{p})^{\pm}$. The transverse flux difference $B^{+}A^{+}\Delta_{x}Q_{ijk}$ is defined as in (30). Note that this term already is computed when approximating the BAq_{xy} term. Next, split this flux difference into waves propagating in the z direction; i.e., solve

$$B^{+}A^{+}\Delta_{x}Q_{ijk} = \sum_{l}\eta^{l}s^{l}. \tag{33}$$

Using this, the update of $\tilde{H}_{i,j+1,k+1}$ reads

$$\tilde{H}_{i,j+1,k+1} := \tilde{H}_{i,j+1,k+1} - \frac{1}{6}\frac{\Delta t}{\Delta x}\frac{\Delta t}{\Delta y}\sum_{l}(\nu^{l})^{+}\eta^{l}s^{l}.$$

To compute all updates in (31), also $B^{-}A^{+}\Delta_{x}Q_{ijk}$ and $B^{\pm}A^{-}\Delta_{x}Q_{ijk}$ need to be split in the z direction. Hence, in addition to the Riemann problems needed in approximating the second-order cross-derivative terms like BAq_{xy}, four new Riemann problems are introduced per interface, by the third-order terms.

The scheme obtained so far is the generalization of the shift and average scheme. The two-dimensional version is identical to the corner transport upwind (CTU) scheme discussed by Colella [7]. The scheme is stable provided

$$\max_{p,q,l}\left(|\lambda^{p}|\frac{\Delta t}{\Delta x}, |\mu^{q}|\frac{\Delta t}{\Delta y}, |\nu^{l}|\frac{\Delta t}{\Delta z}\right) \leq 1, \tag{34}$$

but the scheme is only first-order accurate on smooth solutions.

2.4. The Propagation of the Correction Wave

In this section we look at the propagation of the correction wave, so that the order of accuracy increases. Note that the transverse propagation of the increment waves has already led to terms modeling cross-derivatives needed in a second-order Taylor series expansion.

To obtain full second-order accuracy, it is thus formally necessary to only include the pure second-derivative terms q_{xx}, q_{yy}, and q_{zz}. This is accomplished by propagating the correction waves normal to the interfaces.

However, the resulting second-order accurate method would have very poor stability properties. To maintain good stability properties, we must also perform a transverse propagation of the correction waves in a multidimensional manner. This is developed in this section and then stability analysis is presented in Section 4.

2.4.1. Scalar Equation

We will illustrate the transverse and double transverse propagation of correction waves in the case of scalar advection. First, the correction wave is added as in the one-dimensional case, which gives the terms formally needed for second-order correction but ruins the stability. Again, we present formulas only for the x sweeps, with analogous modifications needed in the other directions:

$$\tilde{F}_{ijk} := \tilde{F}_{ijk} + \frac{1}{2}u\left(1 - u\frac{\Delta t}{\Delta x}\right)\Delta_x Q_{ijk}. \tag{35}$$

The flux (or slope) limiter is applied exactly as in the one-dimensional case; i.e., in (15) and (16), let $\mathcal{W}_i^p = \alpha_i^p = \Delta_x Q_{ijk}$.

To propagate the correction wave in the transverse direction, the natural approach is to move it in the same way as the increment wave (18). Let

$$c(x, t) = (x - x_i + 0.5\Delta x - a(t - t_n))\Delta_x Q_{ij}/\Delta x$$

denote the correction wave associated with cell $C_{i-1,jk}$. (Note that a limited version of $\Delta_x Q_{ijk}$ could be used.) Then we have that

$$
\begin{aligned}
\tilde{G}_{i,j+1,k} &:= \tilde{G}_{i,j+1,k} - \frac{1}{\Delta t}\frac{1}{\Delta z}\frac{1}{\Delta x}\int_{t_n}^{t_{n+1}}\int_{z_k+w(t-t_n)}^{z_{k+1}}\int_{x_i}^{x_i+u(t-t_n)} vc(x, t)\,dx\,dz\,dt, \\
&= \tilde{G}_{i,j+1,k} + uv\frac{\Delta t}{\Delta x}\left(\frac{1}{4} - \frac{1}{6}u\frac{\Delta t}{\Delta x}\right)\Delta_x Q_{ijk} \\
&\quad - uvw\frac{\Delta t}{\Delta z}\frac{\Delta t}{\Delta x}\left(\frac{1}{6} - \frac{1}{8}u\frac{\Delta t}{\Delta x}\right)\Delta_x Q_{ijk}.
\end{aligned}
\tag{36}
$$

With corresponding updates of the $\tilde{H}_{i,j+1,k+1}$ flux, stability is restored. However, the stability is not as good as wanted and the progation of the correction wave has to be done slightly differently in order to obtain (34). Instead of (36), the following update will be used:

$$
\begin{aligned}
\tilde{G}_{i,j+1,k} &:= \tilde{G}_{i,j+1,k} + \frac{1}{2}uv\frac{\Delta t}{\Delta x}\left(1 - u\frac{\Delta t}{\Delta x}\right)\Delta_x Q_{ijk} \\
&\quad - \frac{1}{2}uvw\frac{\Delta t}{\Delta x}\frac{\Delta t}{\Delta z}\left(1 - u\frac{\Delta t}{\Delta x}\right)\Delta_x Q_{ijk}.
\end{aligned}
\tag{37}
$$

Note that only the coefficients are changed. Even if the wave is not advected with the velocity field, it is possible to interpret the update as resulting from a wave propagation. The geometrical interpretation of the total motion of the correction wave is that it consists
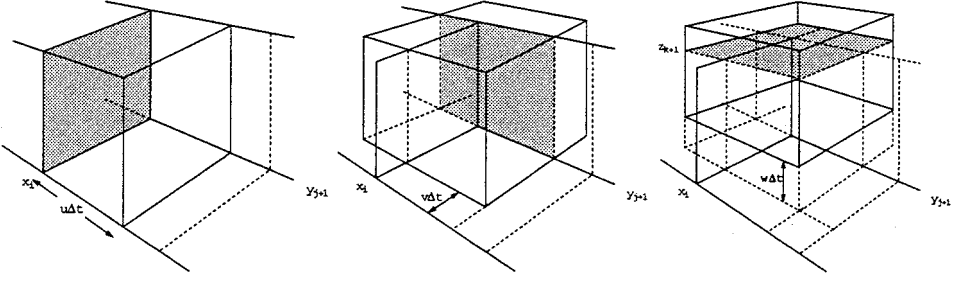
FIG. 3. The propagation of the correction wave when the velocities are positive. The wave is first shifted a distance $u\Delta t$ in the x direction, causing an update of $\tilde{F}_{ijk}$. Next the wave is shifted a distance $v\Delta t$, causing an update of $\tilde{G}_{i-1,j+1,k}$ and $\tilde{G}_{i,j+1,k}$. Finally, the wave is advected a distance $w\Delta t$ in the z direction, causing a update of four $\tilde{H}$ fluxes.

of several steps. In the first step, the wave is moved a distance $u\Delta t$ in the x direction. This results in the familiar 1D update (35). Next, the wave is moved a distance $v\Delta t$ in the y direction (transverse propagation), followed by a final step in which the wave is moved a distance $w\Delta t$ in the z direction (double transverse propagation). These three steps are shown in Fig. 3. Note that also $\tilde{G}$ and $\tilde{H}$ fluxes in the downstream direction are updated. Since there are two coordinate directions covering the transverse propagation, the two last steps above have to be repeated but now in reversed order, i.e., first propagation in z then in y. This will be discussed in more detail below.

2.4.2. *Linear Systems*

As for the scalar example above, the algorithm for propagating the correction wave starts by updating the normal fluxes coordinate-wise,

$$\tilde{F}_{ijk} := \tilde{F}_{ijk} + \frac{1}{2}\sum_{p}|\lambda^{p}|\left(1 - \frac{\Delta t}{\Delta x}|\lambda^{p}|\right)\tilde{\mathcal{W}}_{ijk}^{p}. \tag{38}$$

The limiting is done exactly as in 1D. This is a potential weakness of the method since the limiter only takes into account waves propagating normal to the interfaces. At least for scalar problems there exist ways of doing multidimensional limiting, but they are more expensive to use (e.g., [1, 24, 36, 50]. However, numerical experiments show that this simple one-dimensional limiting is able to control oscillations in a satisfactory way.

Naturally, the 3D propagation of the correction wave has much in common with the propagation of the increment wave. Instead of propagating one wave at the time, a group of waves will be split into waves moving in the transverse direction.

Define

$$\mathcal{S} = \sum_{p}|\lambda^{p}|\left(1 - \frac{\Delta t}{\Delta x}|\lambda^{p}|\right)\tilde{\mathcal{W}}_{ijk}^{p}. \tag{39}$$

This term is to be split in both y and z directions. For example, consider the splitting in the y direction of this correction term into an up-going and a down-going part; i.e., decompose $\mathcal{S}$ as

$$\mathcal{S} = \sum_{q}\varepsilon_{ijk}^{q}w^{q}. \tag{40}$$

The wave $\varepsilon^q_{ijk} w^q$ will update two of the surrounding $\tilde{G}$ fluxes depending on the sign of μ^q. For example,

$$\tilde{G}_{i,j+1,k} = \tilde{G}_{i,j+1,k} + \frac{1}{2}\frac{\Delta t}{\Delta x}\sum_q (\mu^q)^+ \varepsilon^q_{ijk} w^q, \tag{41}$$

$$\tilde{G}_{i-1,j+1,k} = \tilde{G}_{i-1,j+1,k} - \frac{1}{2}\frac{\Delta t}{\Delta x}\sum_q (\mu^q)^+ \varepsilon^q_{ijk} w^q. \tag{42}$$

Down-going waves would instead affect $\tilde{G}_{ijk}$ and $\tilde{G}_{i-1,jk}$. Recall that the flux updates made in the transverse direction consist of the same terms as in the 2D scheme augmented by purely three-dimensional terms. In matrix notation, these two-dimensional updates are

$$\tilde{G}_{i,j+1,k} := \tilde{G}_{i,j+1,k} + \frac{1}{2}\frac{\Delta t}{\Delta x}B^+|A|\left(1 - |A|\frac{\Delta t}{\Delta x}\right)\Delta_x Q_{ijk}$$

$$\tilde{G}_{ijk} := \tilde{G}_{ijk} + \frac{1}{2}\frac{\Delta t}{\Delta x}B^-|A|\left(1 - |A|\frac{\Delta t}{\Delta x}\right)\Delta_x Q_{ijk}$$

$$\tilde{G}_{i-1,j+1,k} := \tilde{G}_{i-1,j+1,k} - \frac{1}{2}\frac{\Delta t}{\Delta x}B^+|A|\left(1 - |A|\frac{\Delta t}{\Delta x}\right)\Delta_x Q_{ijk} \tag{43}$$

$$\tilde{G}_{i-1,jk} := \tilde{G}_{i-1,jk} - \frac{1}{2}\frac{\Delta t}{\Delta x}B^-|A|\left(1 - |A|\frac{\Delta t}{\Delta x}\right)\Delta_x Q_{ijk}.$$

In two dimensions, it is possible to avoid the computation of the eigenvector expansion (or Riemann problem) in (40) by including $\mathcal{S}$ in the 2D part of the flux differences in (22). The proper modifications are

$$A^+\Delta_x Q_{ijk} := A^+\Delta_x Q_{ijk} - \mathcal{S}$$
$$A^-\Delta_x Q_{ijk} := A^-\Delta_x Q_{ijk} + \mathcal{S}. \tag{44}$$

Since $\frac{1}{2}\mathcal{S}$ already is computed in (38), including this transverse propagation requires virtually no extra work.

In two dimensions, the inclusion of the transverse propagation of the correction wave increases neither the order nor the stability limit of the method, but the accuracy may be improved. However, in three dimensions this contribution is essential.

In the three-dimensional case, updates similar to those in (43) must be made to the $\tilde{H}$ fluxes. In matrix notation these terms are

$$\tilde{H}_{ij,k+1} := \tilde{H}_{ij,k+1} + \frac{1}{2}\frac{\Delta t}{\Delta x}C^+|A|\left(1 - |A|\frac{\Delta t}{\Delta x}\right)\Delta_x Q_{ijk}$$

$$\tilde{H}_{ijk} := \tilde{H}_{ijk} + \frac{1}{2}\frac{\Delta t}{\Delta x}C^-|A|\left(1 - |A|\frac{\Delta t}{\Delta x}\right)\Delta_x Q_{ijk}$$

$$\tilde{H}_{i-1,j,k+1} := \tilde{H}_{i-1,j,k+1} - \frac{1}{2}\frac{\Delta t}{\Delta x}C^+|A|\left(1 - |A|\frac{\Delta t}{\Delta x}\right)\Delta_x Q_{ijk} \tag{45}$$

$$\tilde{H}_{i-1,jk} := \tilde{H}_{i-1,jk} - \frac{1}{2}\frac{\Delta t}{\Delta x}C^-|A|\left(1 - |A|\frac{\Delta t}{\Delta x}\right)\Delta_x Q_{ijk}.$$

To compute these updates, the correction term $\mathcal{S}$ must be split in the z direction.

Above we mentioned that there are good reasons for using updates of the form (37) instead of the more intuitive updates (36) resulting from pure advection of the correction wave. The best reason for this is that the stability is increased; cf. Section 4. The updates in (37) are also beneficial for accuracy reasons. Consider the Taylor expansion of q. Due to the large number of terms, we begin by including only terms that arise in the 2D case. Assume that we want to construct a third-order-accurate scheme. Then we have to approximate the following terms:

$$-\frac{1}{6}\Delta t^3(A^3q_{xxx} + A^2Bq_{yxx} + ABAq_{xyx} + AB^2q_{yyx}$$
$$+ BA^2q_{xxy} + BABq_{yxy} + B^2Aq_{xyy} + B^3q_{yyy}). \tag{46}$$

In addition to these terms, we have to approximate terms arising in the truncation error in the approximations of the first- and second-order terms already derived.

For example, the truncation error in the approximation of $\frac{1}{2}\Delta t^2 BAq_{xy}$ is dominated by

$$-\frac{1}{4}\Delta t^2\Delta x(B^+A^+ - B^+A^- + B^-A^+ - B^-A^-)q_{xxy} = -\frac{1}{4}\Delta t^2\Delta xB|A|q_{xxy}. \tag{47}$$

Then approximating

$$\Delta t^2\Delta xB|A|\left(\frac{1}{4} - \frac{1}{6}\frac{\Delta t}{\Delta x}|A|\right)q_{xxy} \tag{48}$$

will cancel the truncation error (47) and add the correct q_{xxy} term from (46). Deriving similar expressions for the rest of the first- and second-order terms yields

$$\frac{1}{6}\Delta t^3ABAq_{xyx} + \Delta t^2\Delta xB|A|\left(\frac{1}{4} - \frac{1}{6}\frac{\Delta t}{\Delta x}|A|\right)q_{xxy} + \Delta t^2\Delta x\left(\frac{1}{4} - \frac{1}{6}\frac{\Delta t}{\Delta x}|A|\right)|A|Bq_{yxx}$$

$$-\frac{1}{6}\Delta t^3BABq_{yxy} + \Delta t^2\Delta xA|B|\left(\frac{1}{4} - \frac{1}{6}\frac{\Delta t}{\Delta x}|B|\right)q_{yyx}$$

$$+ \Delta t^2\Delta x\left(\frac{1}{4} - \frac{1}{6}\frac{\Delta t}{\Delta x}|B|\right)|B|Aq_{xyy} + \frac{1}{6}\Delta t^3A^3q_{xxx} + \frac{1}{6}\Delta t^3B^3q_{yyy}.$$

These terms must be approximated to achieve a third-order scheme. (Note that the update in (36) results in an approximation to only one of these terms that is shown in (48).)

Assume that A and B commute, i.e., that $AB = BA$. Then the expression above, with q_{xxx} and q_{yyy} omitted, reduces to

$$\frac{1}{2}\Delta t^2\Delta xB|A|\left(1 - \frac{\Delta t}{\Delta x}|A|\right)q_{xxy} + \frac{1}{2}\Delta t^2\Delta yA|B|\left(1 - \frac{\Delta t}{\Delta y}|B|\right)q_{yyx}. \tag{49}$$

The transverse propagation of the correction wave as done in (43) yields exactly the desired approximation of the first term in (49). The second term is approximated by the similar transverse propagation of the correction wave emanating from interfaces in the y direction.

For scalar advection with constant coefficients, a third-order-accurate scheme is easily obtained. Once transverse propagation of the correction waves is included, only the terms q_{xxx} and q_{yyy} need to be approximated (cf. [27]).

Finally, consider the purely three-dimensional terms in the update, i.e., terms generalizing the last term in (37). Note that since this update of the $\tilde{G}$ flux contains two Δx and one Δz and these fluxes are differenced in the y direction, the contribution of this term approximates the fourth-order derivative q_{xxzy}.

In a Taylor expansion of the scalar problem, all derivatives of fourth order involving two derivatives in x and one in both y and z add up to

$$-\frac{1}{2}\Delta t^3 \Delta x \, uvw\left(1 - \frac{\Delta t}{\Delta x}u\right)q_{xxyz}. \tag{50}$$

Above, we assumed that the matrices A and B commute, and we do the same here for A, B, and C. Hence, (50) is split evenly between the $\tilde{G}$ fluxes and the $\tilde{H}$ fluxes in the system case; i.e.,

$$-\frac{1}{4}\Delta t^3 \Delta x C B|A|\left(1 - \frac{\Delta t}{\Delta x}|A|\right)q_{xxyz} - \frac{1}{4}\Delta t^3 \Delta x B C|A|\left(1 - \frac{\Delta t}{\Delta x}|A|\right)q_{xxyz}. \tag{51}$$

The first term is approximated by the following flux updates:

$$\tilde{H}_{ij,k+1} := \tilde{H}_{ij,k+1} - \frac{1}{4}\frac{\Delta t}{\Delta x}\frac{\Delta t}{\Delta y}C^+|B||A|\left(1 - |A|\frac{\Delta t}{\Delta x}\right)\Delta_x Q_{ijk}$$

$$\tilde{H}_{ijk} := \tilde{H}_{ijk} - \frac{1}{4}\frac{\Delta t}{\Delta x}\frac{\Delta t}{\Delta y}C^-|B||A|\left(1 - |A|\frac{\Delta t}{\Delta x}\right)\Delta_x Q_{ijk}$$

$$\tilde{H}_{i,j+1,k+1} := \tilde{H}_{i,j+1,k+1} + \frac{1}{4}\frac{\Delta t}{\Delta x}\frac{\Delta t}{\Delta y}C^+B^+|A|\left(1 - |A|\frac{\Delta t}{\Delta x}\right)\Delta_x Q_{ijk}$$

$$\tilde{H}_{i,j+1,k} := \tilde{H}_{i,j+1,k} - \frac{1}{4}\frac{\Delta t}{\Delta x}\frac{\Delta t}{\Delta y}C^-B^+|A|\left(1 - |A|\frac{\Delta t}{\Delta x}\right)\Delta_x Q_{ijk} \tag{52}$$

$$\tilde{H}_{i,j-1,k+1} := \tilde{H}_{i,j-1,k+1} - \frac{1}{4}\frac{\Delta t}{\Delta x}\frac{\Delta t}{\Delta y}C^+B^+|A|\left(1 - |A|\frac{\Delta t}{\Delta x}\right)\Delta_x Q_{ijk}$$

$$\tilde{H}_{i,j-1,k} := \tilde{H}_{i,j-1,k} - \frac{1}{4}\frac{\Delta t}{\Delta x}\frac{\Delta t}{\Delta y}C^-B^-|A|\left(1 - |A|\frac{\Delta t}{\Delta x}\right)\Delta_x Q_{ijk}.$$

In addition to these updates, six additional updates are required in which i is replaced by $i - 1$ in the flux subscripts. The sign of the update is also switched.

Note that these updates involve the same interfaces as the double transverse propagation of the increment wave (31). The updates above require the solution of four additional Riemann problems. But due to the similarities, they may be included in the computation of the double transverse propagation of the increment wave. The proper updates for this inclusion are

$$B^+A^+\Delta_x Q_{ijk} := B^+A^+\Delta_x Q_{ijk} - \frac{3}{2}B^+|A|\left(1 - |A|\frac{\Delta t}{\Delta x}\right)\Delta_x Q_{ijk}$$

$$B^+A^-\Delta_x Q_{ijk} := B^+A^-\Delta_x Q_{ijk} + \frac{3}{2}B^+|A|\left(1 - |A|\frac{\Delta t}{\Delta x}\right)\Delta_x Q_{ijk}$$

$$B^-A^+\Delta_x Q_{ijk} := B^-A^+\Delta_x Q_{ijk} - \frac{3}{2}B^-|A|\left(1 - |A|\frac{\Delta t}{\Delta x}\right)\Delta_x Q_{ijk} \tag{53}$$

$$B^-A^-\Delta_x Q_{ijk} := B^-A^-\Delta_x Q_{ijk} + \frac{3}{2}B^-|A|\left(1 - |A|\frac{\Delta t}{\Delta x}\right)\Delta_x Q_{ijk}.$$

With these changes, both the double-transverse propagation of the increment wave and the correction wave are covered by the updates in (31). Finally, doing similar updates for the $\tilde{G}$ flux will give approximations to the q_{xxzy} term in (51).

Above, it was necessary to assume that the matrices commute when propagating the correction wave in the transverse direction. Note that this only affects (some) third- and fourth-order terms in a Taylor series. Not assuming this would require that a large number of new terms, like $ABAq_{xyx}$, be approximated. This would lead to an extremely complex code, and recall that we are interested in these terms for stability only. We have not been able to find examples in the system case for which the assumption of commuting matrices yields a more restrictive stability limit than the optimal we get for the scalar case.

2.5. Nonlinear Problems and Extensions

So far, only linear problems have been considered. However, by the use of local linearizations, only minor changes have to be made to apply the scheme to nonlinear problems (1). Motivated by the notation used for linear systems, the upwind contribution in (6) reads

$$\Delta_{ijk}^{up} = -\frac{\Delta t}{\Delta x}(\mathcal{A}^+\Delta_x Q_{ijk} + \mathcal{A}^-\Delta_x Q_{i+1,jk}) - \frac{\Delta t}{\Delta y}(\mathcal{B}^+\Delta_y Q_{ijk} + \mathcal{B}^-\Delta_y Q_{i,j+1,k})$$

$$- \frac{\Delta t}{\Delta x}(\mathcal{C}^+\Delta_x Q_{ijk} + \mathcal{C}^-\Delta_z Q_{i,j,k+1}). \tag{54}$$

Here, the terms $\mathcal{A}^+\Delta_x Q_{ijk}$, etc., are to be understood as symbols. The scheme is conservative provided

$$f(Q_{ijk}) - f(Q_{i-1,jk}) = \mathcal{A}^+\Delta_x Q_{ijk} + \mathcal{A}^-\Delta_x Q_{ijk}$$
$$g(Q_{ijk}) - g(Q_{i,j-1,k}) = \mathcal{B}^+\Delta_y Q_{ijk} + \mathcal{B}^-\Delta_y Q_{ijk} \tag{55}$$
$$h(Q_{ijk}) - h(Q_{ij,k-1}) = \mathcal{C}^+\Delta_z Q_{ijk} + \mathcal{C}^-\Delta_z Q_{ijk}.$$

The process of finding the terms $\mathcal{A}^+\Delta_x Q_{ijk}$, etc., so that (55) is satisfied is a form of *flux difference splitting*. In addition, wave strengths $\mathcal{W}_{ijk}^p$ and wave velocities λ_{ijk}^p must be defined so that the flux terms $\tilde{F}_{ijk}$ can be established. Note that waves and velocities are space dependent. There are M_w waves involved, not necessarily equal to the dimension of the system m.

The flux difference splitting and associated waves and velocities may be obtained in different ways. The obvious way is to apply a local linearization that is conservative. A popular choice is the Roe solver [33], where a local approximation A_{ijk} is made to the Jacobian $f'(q)$. This involves finding the state Q_{ijk}^* depending on $Q_{i-1,jk}$ and Q_{ijk} so that if $A_{ijk} = f(Q_{ijk}^*)$ then

$$A_{ijk}(Q_{ijk} - Q_{i-1,jk}) = f(Q_{ijk}) - f(Q_{i-1,jk}). \tag{56}$$

This property ensures conservation. The waves $\mathcal{W}_{ijk}^p$ and associated speeds λ_{ijk}^p are derived exactly as in the linear case. A matrix satisfying (56) is found for several important systems like the Euler equations of gas dynamics.

Since the solution only consists of discontinuities, rarefaction waves may cause problems. If these waves are transonic, i.e., involve both positive and negative velocities, the numerical

solution may contain physically incorrect shocks. To correct this, an entropy fix should be applied [17, 25, 35].

In the linear case, it is reasonable to compare wave strengths α_i^p (16) from neighboring interfaces, since the eigenvectors r^p are constants. In the nonlinear case, the waves $\mathcal{W}_{i-1,jk}^p$, $\mathcal{W}_{ijk}^p$, and $\mathcal{W}_{i+1,jk}^p$ are not in general parallel, as vectors in $\mathbb{R}^m$. In CLAWPACK, the default limiting is based on a projection of $\mathcal{W}_{i\pm1,jk}^p$ onto $\mathcal{W}_{ijk}^p$. The lengths of these projections are compared to the length of $\mathcal{W}_{ijk}^p$. The limiting is performed according to

$$\tilde{\mathcal{W}}_{ijk}^p = \Phi\left(\theta_{ijk}^p\right)\mathcal{W}_{ijk}^p,$$

$$\theta_{ijk}^p = \begin{cases} \left(\mathcal{W}_{i-1,jk}^p, \mathcal{W}_{ijk}^p\right)/\left(\mathcal{W}_{ijk}^p, \mathcal{W}_{ijk}^p\right), & \lambda_{ijk}^p > 0 \\ \left(\mathcal{W}_{i+1,jk}^p, \mathcal{W}_{ijk}^p\right)/\left(\mathcal{W}_{ijk}^p, \mathcal{W}_{ijk}^p\right), & \lambda_{ijk}^p < 0, \end{cases}$$

where $(\cdot, \cdot)$ represents the inner product in $\mathbb{R}^m$. Note that this limiting generalizes the limiting used on linear systems, i.e., (15) and (16).

We have used Roe-type Riemann solvers for the Euler equations in the computations presented here. There exist many other ways of defining the flux difference splitting and associated waves that can also be used in our formulation. In some situations it might be advantageous to use the exact solution of the Riemann problem. For example, when applied to the Euler equations, the Roe solver may produce negative pressure if the jump is large enough. Assume that Q_{ijk}^0, the exact solution for $x = x_i$, has been found. Then the flux splitting can be defined as

$$\mathcal{A}^+\Delta_x Q_{ijk} = f(Q_{ijk}) - f\left(Q_{ijk}^0\right)$$
$$\mathcal{A}^-\Delta_x Q_{ijk} = f\left(Q_{ijk}^0\right) - f(Q_{i-1,jk}).$$

The waves and the associated velocities needed for the correction waves also must be specified. The states in the exact Riemann solution naturally define the jumps $\mathcal{W}_{ijk}^p$. If the original waves are discontinuities, the velocities should be chosen according to the Rankine–Hugoniot condition. If the waves are rarefaction waves, an average velocity could be used.

A third approach is worth considering: a hybrid version in which the exact solver defines the flux splitting, and the Roe solver defines the waves and velocities.

Transverse and double transverse propagations of increment and corrections waves are accomplished by constructing matrices B_{ijk} and C_{ijk}. These matrices are simply taken as the Jacobians $g'(q)$ and $h'(q)$, respectively, evaluated at a state "close" to $Q_{i-1,jk}$ and Q_{ijk}. A good choice is to use the Roe-averaged state Q_{ijk}^* already computed in the construction of the flux difference splitting.

Each product between a matrix and a vector corresponds to a Riemann problem. While an entropy fix may be necessary for the flux difference splitting, computations indicate that there is no need for this correction in the transverse direction. Hence, the Riemann problems used in computing these flux updates require less work than the Riemann problems in the normal direction. No entropy fix is needed, and the state used in evaluating the Jacobians is already computed.

A family of wave propagation schemes is defined by how the increment waves and correction waves are propagated. The order, accuracy, and stability depend on how the waves are treated. It is useful to establish a notation refering to how the propagation is done.

Let a specific scheme be defined by the three parameters (m_1, m_2, m_3), where the integers m_1, m_2, m_3 have the following meanings:

$$m_1 = \begin{cases} 1 & \text{The second order correction wave is not included;} \\ & \quad \text{thus the method is formally first-order accurate.} \\ 2 & \text{The correction wave is included.} \end{cases}$$

$$m_2 = \begin{cases} 0 & \text{No transverse propagation.} \\ 1 & \text{Transverse propagation of the increment wave.} \\ 2 & \text{Transverse propagation of both increment and} \\ & \quad \text{correction wave (requires } m_1 = 2\text{).} \end{cases}$$

$$m_3 = \begin{cases} 0 & \text{No double transverse propagation.} \\ 1 & \text{Double transverse propagation of the increment wave (requires } m_2 > 0\text{).} \\ 2 & \text{Double transverse propagation of both increment and} \\ & \quad \text{correction wave (requires } m_2 = 2\text{).} \end{cases}$$

For example, Method (1, 1, 0) defines the first-order scheme in which the increment wave moves as in 2D. The complete wave propagation method is Method (2, 2, 2). (In CLAWPACK, m_2 and m_3 are specified by a two-digit integer; hence, the method is identified by only two parameters m_1 and $10 \cdot m_2 + m_3$.)

The number of Riemann problems needed increases as the propagation becomes more and more complex. In the first-order donor-cell method, i.e., Method (1, 0, 0), only one Riemann problem must be solved per interface. If the increment wave moves as in the 2D case (Method (1, 1, 0)), four additional problems must be solved. The generalization of the shift and average scheme, i.e., Method (1, 1, 1), requires a total of 13 Riemann problems. Five Riemann problems must be solved per interface for (the unconditionally unstable) Method (2, 1, 0). The simple generalization of the full 2D wave propagation scheme, Method (2, 2, 0), requires seven Riemann problems. This number may be reduced to five as noted above. The shift and average scheme, plus propagation normal to the interface of the correction wave (Method (2, 1, 1)), requires the solution of 15 Riemann problems per interface. The same number is required for Method (2, 2, 2), the full three-dimensional wave propagation scheme.

The total number of Riemann problems needed per cell is three times the number per interface. This indicates that the 3D wave propagation methods may be computationally expensive, depending on the choice of Riemann solver. Using the Roe-solver approach, only one of the Riemann problems, per interface, requires the entropy fix and computation of the Roe-average state. The rest of the Riemann problems involve significantly less work, essentially just a matrix–vector multiply to decompose a vector into eigencomponents.

The advantage of using (6) with the flux difference splitting (55) in the definition of the upwind term Δ_{ijk}^{up} is that the flux functions are not explicitly needed. As a conceqence, the same scheme is applicable to a larger class of quasilinear hyperbolic problems of the form (3). The matrices may depend on x, y, z, and t in addition to the solution q. In the "flux difference splitting" (which is called "fluctuation splitting" more generally in [28]), the waves and associated velocities are easily defined. However, note that spacially varying matrices may result in reflections in addition to transmission of waves across cell interfaces. This complicates the problem, but may still be treated within the same framework; cf. [28] for details.

3. APPLICATIONS

In this section we consider the Euler equations which model an inviscid, compressible, and non-heat-conducting gas. The system may be written as

$$
\begin{bmatrix} \rho \\ \rho u \\ \rho v \\ \rho w \\ E \end{bmatrix}_t + \begin{bmatrix} \rho u \\ \rho u^2 + p \\ \rho uv \\ \rho uw \\ u(E + p) \end{bmatrix}_x + \begin{bmatrix} \rho v \\ \rho uv \\ \rho v^2 + p \\ \rho vw \\ v(E + p) \end{bmatrix}_y + \begin{bmatrix} \rho w \\ \rho uw \\ \rho vw \\ \rho w^2 + p \\ w(E + p) \end{bmatrix}_z = 0, \qquad (57)
$$

where ρ and p denote the density and pressure. The velocity components in the x, y, and z directions are u, v, and w, respectively. If we assume that the gas is polytropic, the total energy density E is

$$
E = \frac{1}{2}\rho\left(u^2 + v^2 + w^2\right) + \frac{1}{\gamma - 1}p,
$$

where γ is a gas constant taken to be 1.4 in the examples below.

The Roe approximate Riemann solver is used in all the following examples. Thus, the Jacobian matrices are evaluated at a specific state, as described in Section 2, in order to ensure conservation and to define the waves needed in the algorithm. For details on this see [33] and the Riemann solver routines in the CLAWPACK software [29]. In [28], the details concerning the solution of the two-dimensional isothermal equations are given. We refer to that paper, since the main principles are the same, when it comes to defining matrices and flux splitting, as in the three-dimensional full Euler case.

3.1. Smooth Euler Solution

To verify second-order convergence, we consider an initial value problem with a smooth solution, at least for the time interval considered. Initially, the gas is at rest and

$$
\rho(x, y, z, 0) = E(x, y, z, 0) = 1 + 0.1e^{-30(r-1)^2},
$$

where $r = \sqrt{x^2 + y^2 + z^2}$. The solution will remain spherically symmetric. Due to this, it is possible to formulate (57) as a one-dimensional conservation law with a source term,

$$
\begin{bmatrix} \rho \\ \rho u \\ E \end{bmatrix}_t + \begin{bmatrix} \rho u \\ \rho u^2 + p \\ u(E + p) \end{bmatrix}_r = -\frac{1}{r}\begin{bmatrix} \rho u \\ \rho u^2 \\ u(E + p) \end{bmatrix}. \qquad (58)
$$

Here, u denotes the radial velocity. An accurate reference solution is obtained by solving this equation using one-dimensional CLAWPACK routines. Due to the symmetry, the computational domain for the three-dimensional scheme can be taken to be a single octant $(x, y, z) \in [0, 2] \times [0, 2] \times [0, 2]$. At the boundaries $x = 0$, $y = 0$, and $z = 0$, symmetric boundary conditions are used. The remaining boundaries are all of the outflow type described in [28].

TABLE I

Errors for the Smooth Euler Problem Computed with Method (1, 1, 1) on a $N \times N \times N$ Grid

	1-norm errors			Max-norm errors		
N	ρ	ρu	E	ρ	ρu	E
20	6.482×10^{-3}	2.498×10^{-3}	9.425×10^{-3}	9.398×10^{-3}	7.496×10^{-3}	1.373×10^{-2}
40	3.492×10^{-3}	1.338×10^{-3}	5.074×10^{-3}	5.292×10^{-3}	4.389×10^{-3}	7.738×10^{-3}
80	1.831×10^{-3}	7.003×10^{-4}	2.658×10^{-3}	2.729×10^{-3}	2.350×10^{-3}	3.984×10^{-3}
Order	0.93	0.93	0.93	0.96	0.90	0.96

Note. The errors in ρv and ρw equal the errors in ρu. The convergence order is estimated on the two finest grids.

Boundary conditions are imposed in exactly the same way as described in [28] for one and two dimensions: two additional rows of "ghost cells" along each edge are introduced. Values in the ghost cells are set in each time step in such a way as to give the correct behavior. Zero-order extrapolation is used at the outflow boundaries while reflection is used at the symmetry planes.

The solution is computed on an $N \times N \times N$ grid at time $t = 0.5$. In Table I, the errors for Method (1, 1, 1) are given for $N = 20$, 40, and 80. The errors are computed by comparing them with the one-dimensional reference solution. The rate of convergence is estimated using the two finest grids according to the formula

$$\text{convergence order} = \frac{1}{\ln 2} \ln\left(\frac{\text{error}(\Delta x)}{\text{error}(\Delta x/2)}\right).$$

The errors in ρv and ρw equal the errors in ρu. As expected, this scheme is approximately first-order accurate. In Table II, the errors for the full wave propagation scheme Method (2, 2, 2) are given. Since the solution is smooth, no limiting is performed. According to the figures in this table, the scheme is second-order accurate on this problem. In Fig. 4, scatter plots of the density using $N = 20$ and $N = 40$ are shown. Every value in the $N \times N \times N$ grid is plotted against r, the distance from the origin. The solid curve corresponds to the reference solution. In the computations for both the first- and second-order scheme, fixed time steps $\Delta t = \Delta x = 2/N$ are used giving a Courant number of approximately 0.78.

TABLE II

Errors for the Smooth Euler Problem Computed with Method (2, 2, 2) on a $N \times N \times N$ Grid

	1-norm errors			Max-norm errors		
N	ρ	ρu	E	ρ	ρu	E
20	4.334×10^{-3}	1.705×10^{-3}	6.290×10^{-3}	6.985×10^{-3}	5.140×10^{-3}	1.012×10^{-2}
40	1.361×10^{-3}	4.767×10^{-4}	1.961×10^{-3}	2.331×10^{-3}	1.761×10^{-3}	3.368×10^{-3}
80	3.541×10^{-4}	1.254×10^{-4}	5.091×10^{-4}	6.387×10^{-4}	4.931×10^{-4}	9.216×10^{-4}
Order	1.94	1.93	1.95	1.87	1.84	1.87

Note. The errors in ρv and ρw equal the errors in ρu. The convergence order is estimated on the two finest grids.
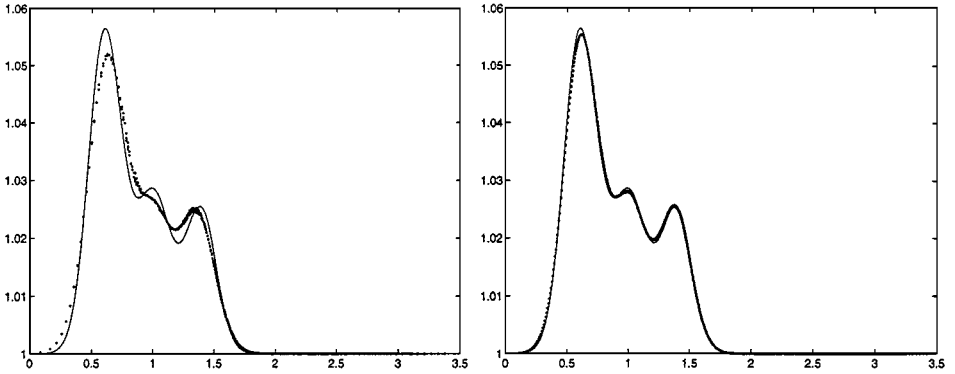
FIG. 4. Scatter plots for the Euler equation with a smooth solution, computed with Method (2, 2, 2). The density is depicted against the distance from origin. In the left picture, $N = 20$, while in the right picture $N = 40$. The solid curve is the reference fine-grid solution from a one-dimensional spherically symmetric calculation.

3.2. A Spherical Riemann Problem

In this example we consider a spherical Riemann problem between two parallel walls at $z = 0$ and $z = 1$. Initially the gas is at rest with density and pressure $\rho_{out} = 1$ and $p_{out} = 1$ everywhere except in a sphere centered at $(0, 0, 0.4)$ with radius 0.2. Inside the sphere $\rho_{in} = 1$ and $p_{in} = 5$. The jump in pressure results in a strong outward moving shock wave and contact discontinuity and an inward moving rarefaction wave. This inward moving wave causes a local "implosion," and a second outward moving shock wave is created. The main features of the solution are the interactions between these waves and between waves and the walls. Another significant feature is the development of a near stationary low-density region in the center of the domain. Until the initial shock wave reaches the lower wall, the solution is spherically symmetric. After this, the solution will remain cylindrically symmetric. Hence, it is possible to formulate this as a two-dimensional problem with a source term,

$$
\begin{bmatrix} \rho \\ \rho u \\ \rho w \\ E \end{bmatrix}_t + \begin{bmatrix} \rho u \\ \rho u^2 + p \\ \rho u w \\ u(E + p) \end{bmatrix}_r + \begin{bmatrix} \rho w \\ \rho u w \\ \rho w^2 + p \\ w(E + p) \end{bmatrix}_z = -\frac{1}{r} \begin{bmatrix} \rho u \\ \rho u^2 \\ \rho u w \\ u(E + p) \end{bmatrix}, \qquad (59)
$$

where u now denotes the radial velocity in the x–y plane. This equation is solved using two-dimensional CLAWPACK routines, and the results are used for comparison. The two-dimensional problem is solved on a 600×400 grid. Due to the symmetry, the computational domain is $(r, z) = [0, 1.5] \times [0, 1]$, where $r = \sqrt{x^2 + y^2}$. Figure 5 shows a schlieren picture of the solution at $t = 0.7$. This picture emulates a photographic technique used in physical experiments. The magnitude of the density gradient is depicted. The larger the gradient, the darker the region. Strong nonlinear shading is used to enhance weak structures in the flow. In this figure, the symmetric part is also depicted. Note the strong contact discontinuity surrounding the low-density region near the center. There is also an nonphysical feature visible near the center of the domain. It is caused by the wave focusing and is highly grid dependent. Due to the nonlinear shading in this schlieren image, the magnitude of this feature is exaggerated. Its influence on the rest of the flow field is actually very weak.
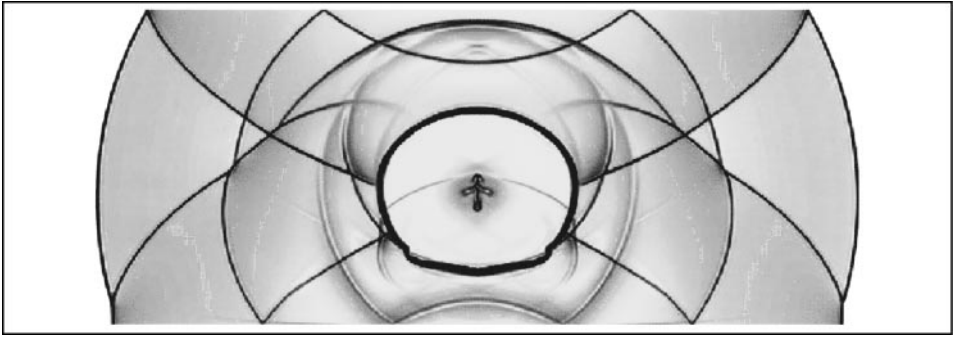
FIG. 5. A schlieren type image showing the density at $t = 0.7$. The two-dimensional axisymmetric problem has been solved using a 600×400 grid on half the domain ($0 \leq x \leq 1.5$, $0 \leq y \leq 1$) and reflected to $-1.5 \leq x \leq 0$.

Due to the symmetry, the computational domain for the three-dimensional algorithm is $(x, y, z) \in [0, 1.5] \times [0, 1.5] \times [0, 1]$. In Fig. 6, the pressure in the x–z plane at $t = 0.7$ is shown using an increasing number of cells. The solution is computed using Method (2, 2, 2). The two-dimensional results are also given for comparison.

Another way of graphically indicating convergence is to consider scatter plots, like those used in the previous example. In Fig. 7, the pressure is plotted against the distance from the z axis. The plane used is $z = 0.4$ at $t = 0.7$. These pictures indicate not only that the main features are well resolved, but also that the finer structures appear to be converging. In both
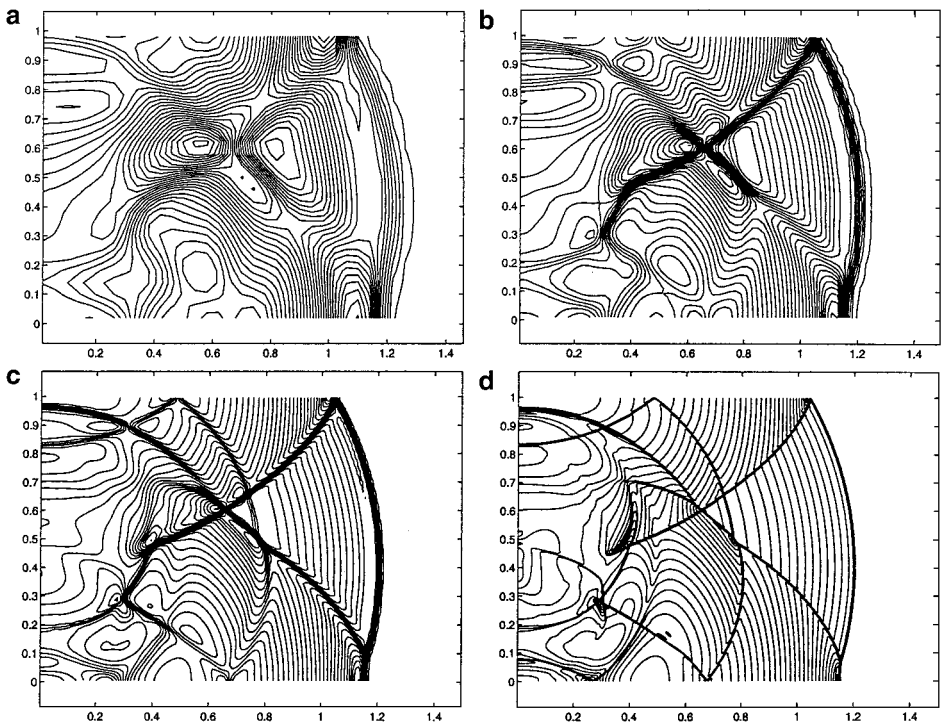
FIG. 6. The pressure in the x–z plane at $t = 0.7$ computed on different grids: (a) $37 \times 37 \times 25$, (b) $75 \times 75 \times 50$, (c) $150 \times 150 \times 100$. In (d), results from the corresponding 2D computation using a 600×400 grid are shown.
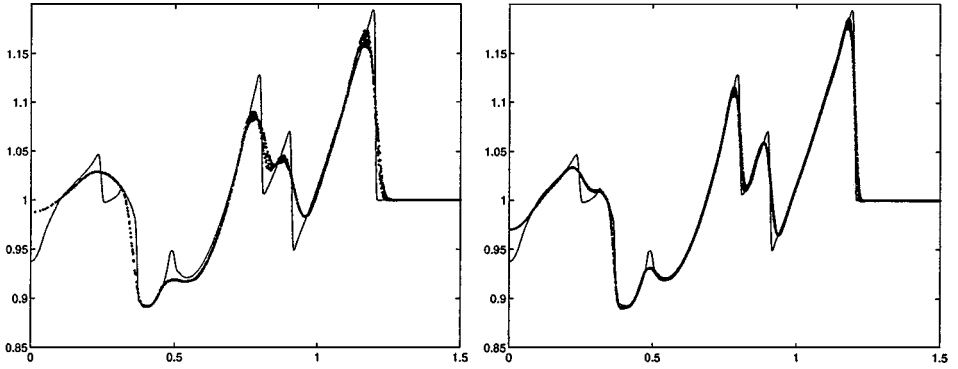
FIG. 7. Scatter plots of the pressure versus the distance from the z axis in the plane $z = 0.4$. In the left picture the computational grid is $75 \times 75 \times 50$, while in the right a $150 \times 150 \times 50$ grid is used. The solid curve corresponds to the 600×400 2D computation.

the two-dimensional and the three-dimensional computations, MC limiters are used on all waves. In these computations the Courant number was approximately 0.9.

Additional images and animations from both the 2D and 3D computations may be found on the Web page [20].

3.3. Vorticity Generated by a Shock Wave

As an example of a pure three-dimensional problem, we consider the situation where shocks interact with variable density regions. One practical application of such problems is the study of how vorticity produced by these interactions mixes two different gases. The problem is often simplified by considering a single planar wave hitting a cylindrical or spherical region containing a different gas; cf. [10, 30]. In these papers a two-component gas is considered. Here, we only consider a single-component gas.

Initially, the gas is at rest. The pressure and the density equal unity everywhere, except for two cylindrical regions perpendicular to each other. Both cylinders contain constant state gas. The radius of each cylinder is $r = 0.2$. In the cylinder along the z axis, i.e., with symmetry axis $x = y = 0$, the density is $\rho = 1$ but the pressure is $p = 10$, and thus cylindrically shaped shock waves will emanate from this cylinder due to the overpressure. The other cylinder is parallel to the y axis, with symmetry axis $x = 0.4$ and $z = 0$. In this cylinder, the pressure is $p = 1$, but the density is lower, $\rho = 0.1$. The resulting contact discontinuty is stationary until it is disturbed by the shock waves. The initial set up is depicted in Fig. 8a.

The experiment is set up in such a way that as the front shock hits the low-density cylinder, a huge amount of vorticity is produced. Let $\vec{\omega} = \nabla \times \vec{u}$ denote the vorticity. The vorticity equation reads

$$\frac{\partial \vec{\omega}}{\partial t} = \nabla \times (\vec{u} \times \vec{\omega}) + \frac{\nabla \rho \times \nabla p}{\rho^2}. \tag{60}$$

The last term on the right-hand side is called the baroclinic source term and is responsible for the vorticity production.

As the shock wave propagates through the low-density region, the latter winds up into two rotating regions (or rolls). The contact discontinuity resulting from the high-pressure region
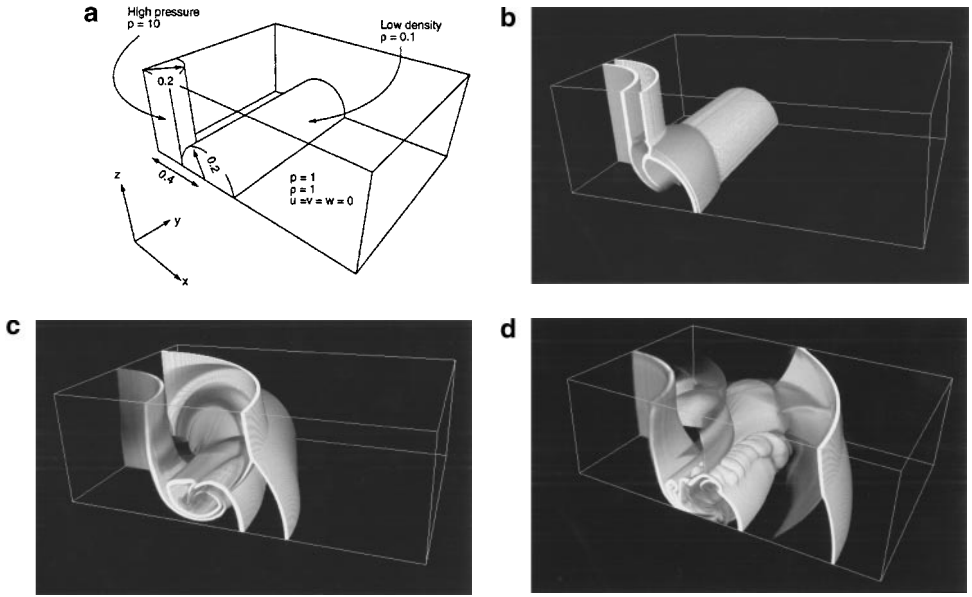
FIG. 8. (a) The initial condition. The rest of the images depict the quanity $|\nabla\rho|$, also used in schlieren pictures, at different times: (b) $t = 0.1$, (c) $t = 0.3$, (d) $t = 0.5$.

will also be rolled up in this vortical motion. The upper roll rotates counter-clockwise, while the one below rotates in the clockwise direction. These two regions will after some time interact. Another vortical feature is the formation of vortex tubes on the envelope of the rolls. This is a pure three-dimensional feature and creates a periodic pattern in the length direction of the low-density region. These vortex tubes will become stretched due to the motion of the rolls and eventually burst, resulting in a turbulent looking region. The shock wave has passed a long time before the flow reaches this state. In the early state of the shock interaction, the part of the wave that penetrates the low-density region speeds up due to the increased sound speed. This results in a splitting of the shock wave.

The computational domain is $[0, 1.5] \times [0, 1] \times [0, 0.5]$, and symmetry is assumed across the planes $x = 0$, $y = 0$, and $z = 0$. Due to the turbulent-like behavior, the symmetry assumption is not correct, but is selected to get a manageable grid size. The computation is performed on a $300 \times 200 \times 100$ grid with Method (2, 2, 2), and the MC limiter is used. As expected, the details in the vortex dynamics depend on the limiter used, and the results in this region should only be taken qualitatively.

In Fig. 8, the solution is shown at different times. Details on the quantities depicted and techniques used are described below. At $t = 0.1$ (Fig. 8b), the incident shock wave has partially encapsulated parts of the low-density cylinder. The two essentially cylindrical surfaces are, from the left, the contact surface and the shock wave. Note that this part of the shock wave has a lower speed than the one encapsulating the low-density cylinder. As mentioned above, this is due to the increased sound speed inside this cylinder. Also note that the low-density cylinder has started to collapse due to the interaction with the shock wave. In Fig. 8c, at $t = 0.3$, the roll has become more visible. Note that the incident shock wave has passed this vortex in most of the computational domain, and that the interaction has created a triple shock configuration. In Fig. 8d, ($t = 0.5$), the periodic pattern on the envelope of the roll is seen. Inside each of these finger-shaped regions, there is a loop of
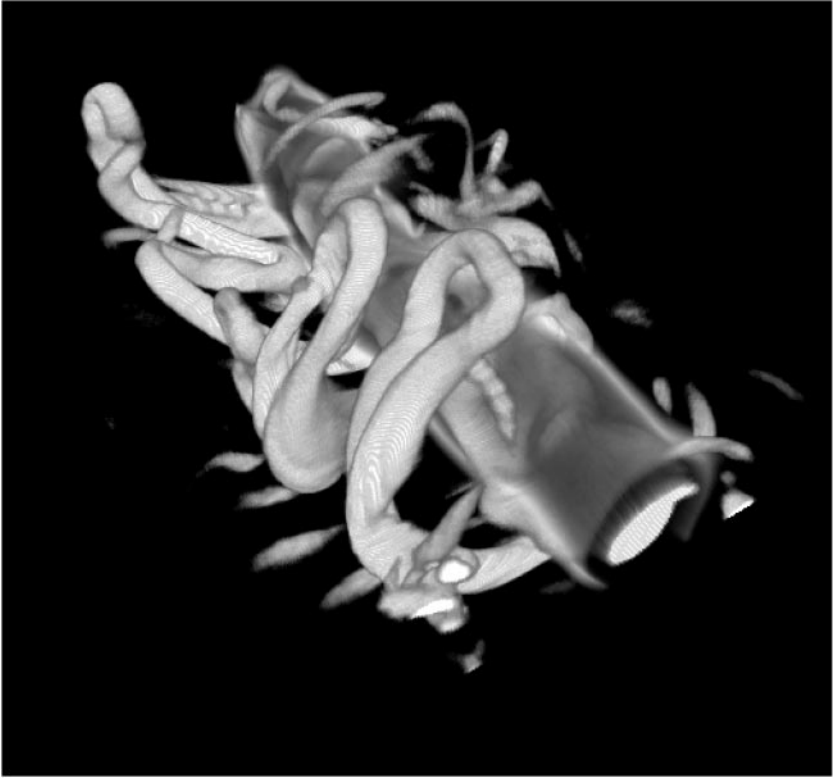
FIG. 9. A subset of the computational domain shown at $t = 0.8$. Both enstrophy and (low) pressure are visualized in this picture.

smaller vortex tubes. (This is illustrated more clearly at a later time in Fig. 9). The weak shock located at the top of the roll is an implosion shock, similar to the one that appeared in the previous example.

The images in Fig. 8 were produced using the visualization tool Viz [51], freely available for noncommersial use. Viz is a highly interactive tool for displaying large voxel-based data sets. It was initially created to utilize the potential of hardware accelerated 3D textures. The voxel may be thought of as a single cell in a regular grid, including information on the solution value (or color) and the associated opacity. Due to the possibility of adding opacity to the dataset, a range of values can be studied, in contrast to the more common iso-surface technique.

When using volume graphics for visualizing shock structures, very little needs to be done as long as the schlieren quantity $\mathcal{S} = |\nabla \rho|$ is used. Typically, the opacity map is monotonic, starting with zero opacity in a neighborhood of $\mathcal{S} = 0$. Then it increases to full opacity in another relatively small region. In the region where the opacity increases, the value V in the HSV color model should also change, typically from darker to brighter, to add some contrast to the image. (In the HSV model, a color is specified by its hue (H), its purity or saturation (S), and its lightness or value (V)). This simple, and very easy to use approach, is used for making Figs. 8b–d. An isosurface-like image is shown, but there is no need to specify discrete values of $\mathcal{S}$. All discontinuities are visible, except for those very weak ones that may hide in the $\mathcal{S}$ range, where zero opacity is specified. Note that due to the change in value V and opacity, weaker discontinuities appear to be darker and more transparent.

In Fig. 9, another application of voxels graphics and Viz is shown. The time is $t = 0.8$ and only a subset of the data is shown, centered along the roll. Two scalar fields are displayed in the same scene. To visualize the smaller vortex tubes on the envelope of the roll, the enstrophy is used, i.e., $|\vec{\omega}|^2$. Note that the surfaces of these tubes are made darker to enhance the shape of these features. The other quantity shown is the dominating low-pressure region. In contrast to the enstrophy, the surface of this region is made lighter. Animations and additional (color) images from this computation may be found on the Web page [20].

4. STABILITY

In this section we investigate the stability properties of the algorithms introduced in Section 2 applied to linear problems. Initially we study the case with no limiter, so that the numerical scheme itself is linear and we can use the von Neumann analysis. In Section 4.4 we also investigate the effect of limiters by running the algorithm and calculating amplification factors for different sets of initial data. This is of interest because we have found that some methods which are unstable without limiters due to exponential growth of high-frequency components are stabilized by the use of limiters.

We consider the scalar advection equation with constant coefficients in Section 4.1. The linearized Euler equations have also been studied and we found that the algorithms have similar stability properties in each case.

For a general linear system $q_t + Aq_x + Bq_y + Cq_z = 0$ in which the matrices A, B, C have eigenvalues λ^p, μ^q, and ν^l, respectively, we define the *directional Courant numbers* as

$$\omega_1 = \frac{\Delta t}{\Delta x}\max_p|\lambda^p|, \quad \omega_2 = \frac{\Delta t}{\Delta y}\max_q|\mu^q|, \quad \omega_3 = \frac{\Delta t}{\Delta z}\max_l|\nu^l|, \tag{61}$$

and set $\vec{\omega} = (\omega_1, \omega_2, \omega_3)$, not to be confused with the vorticity in the previous section. The Courant number is the maximum of these three quantites. The best we can hope for with methods of the type developed here is that they will be stable for all Courant numbers up to 1, i.e., for

$$\max(\omega_1, \omega_2, \omega_3) \leq 1. \tag{62}$$

This set is a cube in ω_1–ω_2–ω_3 space. For most methods the stability restriction is most severe along the diagonal of the cube, i.e., for the special case where $\omega_1 = \omega_2 = \omega_3$, and it is often possible to obtain analytic expressions for the amplification factor in this special case. When this case is considered we will denote the common value of $\vec{\omega}$ by ω_d,

$$\omega_d \equiv \omega_1 = \omega_2 = \omega_3, \quad \text{along the diagonal.}$$

Von Neumann analysis is based on inserting the Fourier mode

$$Q_{IJK} = e^{i(\xi I + \eta K + \theta K)} \tag{63}$$

into the numerical scheme. We use capital letters IJK as the grid index here to avoid confusion with $i = \sqrt{-1}$. For a linear method on a linear problem, this will result in an

expression of the form

$$\bar{Q}_{IJK} = T(\xi, \eta, \theta, \vec{\omega}) Q_{IJK}, \tag{64}$$

where $\bar{Q}$ denotes the numerical solution at the next time step. For scalar advection, T is a scalar. For a system of m equations, T is an $m \times m$ matrix. In the scalar case, the method is stable for given $\vec{\omega}$ if

$$\mathcal{T}(\vec{\omega}) \equiv \max_{\xi, \eta, \theta} |T(\xi, \eta, \theta, \vec{\omega})| \leq 1, \tag{65}$$

where maximum is taken for $-\pi \leq \xi, \eta, \theta \leq \pi$. In fact for all the methods considered, $T(0, 0, 0, \vec{\omega}) = 1$ for all $\vec{\omega}$, so (65) will be satisfied with equality in the stability region.

Only in simple cases is it possible to obtain analytic expressions for $\mathcal{T}(\vec{\omega})$. The diagonal case where $\vec{\omega} = \vec{\omega}_d \equiv (\omega_d, \omega_d, \omega_d)$ will be denoted by $\mathcal{T}(\vec{\omega}_d)$. In most cases we must estimate $\mathcal{T}(\vec{\omega})$ or $\mathcal{T}(\vec{\omega}_d)$ numerically by calculating $T(\xi, \eta, \theta, \vec{\omega})$ over a discrete set of ξ, η, θ values in the cube $-\pi \leq \xi, \eta, \theta \leq \pi$ and take the maximum over these values. This was done for two-dimensional analysis in [27].

For a system of equations, when T is a matrix, the method is stable at some $\vec{\omega}$ if T is diagonalizable and the spectral radius $r(T)$ is no larger than 1. For the class of wave propagation schemes considered, the amplification matrix is not proved to be diagonalizable. For those problems we have considered, numerical studies indicate that T has this property in major parts of the wavenumber domain. For those wavenumbers where the matrix is indicated to be nondiagonalizable, $\|T^n\|$ is computed for different values of n. In these cases, $\|T^n\|$ stays nicely bounded, and the spectral radius is always less than unity. Based on these observations, the wave propagation schemes is said to be stable for given $\vec{\omega}$ if

$$\mathcal{T}(\vec{\omega}) \equiv \max_{\xi, \eta, \theta} r(T(\xi, \eta, \theta, \vec{\omega})) = 1,$$

where maximum is taken for $-\pi \leq \xi, \eta, \theta \leq \pi$. In general, this is only a necessary condition for stability in the system case, but we have not observed that it fails for our applications.

4.1. Scalar Advection

Consider the advection equation (4), where u, v, and w are positive constants. The directional Courant numbers are then

$$\omega_1 = u \frac{\Delta t}{\Delta x}, \quad \omega_2 = v \frac{\Delta t}{\Delta y}, \quad \omega_3 = w \frac{\Delta t}{\Delta z}.$$

As an example of this stability analysis, consider the donor-cell upwind method

$$\bar{Q}_{IJK} = Q_{IJK} - \omega_1(Q_{IJK} - Q_{I-1,JK}) - \omega_2(Q_{IJK} - Q_{I,J-1,K}) - \omega_3(Q_{IJK} - Q_{IJ,K-1})$$

$$= Q_{IJK} - \omega_1 \Delta_x Q_{IJK} - \omega_2 \Delta_y Q_{IJK} - \omega_3 \Delta_z Q_{IJK},$$

where Δ_x, Δ_y, Δ_z denote the upwind difference operators. This is the wave propagation Method $(1, 0, 0)$ from Section 2. Inserting the Fourier mode (63) into this method yields $T(\xi, \eta, \theta, \vec{\omega})$:

$$T^{100} = 1 - \omega_1(1 - e^{-i\xi}) - \omega_2(1 - e^{-i\eta}) - \omega_3(1 - e^{-i\theta}).$$

TABLE III
The Amplification Factor $\mathcal{T}(\vec{\omega}_d)$ versus the CFL Number $\omega_d = \omega_1 = \omega_2 = \omega_3$
for the Scalar Problem

| ω_d | $\max_{\xi,\eta,\theta}\lvert T\rvert$ for | | | | | | | | |
	T^{100}	T^{110}	T^{111}	T^{210}	T^{211}	T^{220}	T^{221}	T^{222}	LW
0.1	1.00	1.00	1.00	1.06	1.05	1.00	1.00	1.00	1.00
0.2	1.00	1.00	1.00	1.24	1.18	1.00	1.00	1.00	1.00
0.3	1.00	1.00	1.00	1.54	1.32	1.00	1.00	1.00	1.03
0.4	1.40	1.00	1.00	1.96	1.45	1.00	1.00	1.00	1.17
0.5	2.00	1.00	1.00	2.50	1.50	1.00	1.50	1.00	1.57
0.6	2.60	1.72	1.00	3.16	1.43	1.06	2.02	1.00	2.21
0.7	3.20	2.68	1.00	3.94	1.26	1.37	2.33	1.00	3.01
0.8	3.80	3.88	1.00	4.84	1.11	2.00	2.33	1.00	3.97
0.9	4.40	5.32	1.00	5.86	1.02	3.92	1.92	1.00	5.08
1.0	5.00	7.00	1.00	7.00	1.00	7.00	1.00	1.00	6.32
1.01	5.06	7.18	1.06	7.12	1.12	7.37	1.14	1.12	6.45

Here and below the superscripts on T and $\mathcal{T}(\vec{\omega})$ refer to the labels (m_1, m_2, m_3) denoting the method. This donor-cell method can be shown to be stable only when

$$\omega_1 + \omega_2 + \omega_3 \leq 1,$$

which is more restrictive than our desired bound (62). In particular, along the diagonal we find that

$$\mathcal{T}(\vec{\omega}_d) = \max(1, \lvert 1 - 6\omega_d \rvert),$$

so that the method is only stable for $\omega_d \leq 1/3$.

In Table III we present the values of $\mathcal{T}(\vec{\omega}_d)$ found numerically for each method of the type presented in Section 2, and also for the classical Lax–Wendroff method. The column labeled T^{100}, for example, shows that the method is stable for $\omega_d = 0.3$ but not for $\omega_d = 0.4$, since in the latter case the amplification factor is 1.40.

We can improve the stability properties of the upwind algorithm by moving up to Method $(1, 1, 0)$, in which we introduce transverse propagation of the increment waves into adjacent cells. The amplification factor is then

$$T^{110} = T^{100} + \omega_1\omega_2(1 - e^{-i\xi})(1 - e^{-i\eta}) + \omega_1\omega_3(1 - e^{-i\xi})(1 - e^{-i\theta})$$
$$+ \omega_2\omega_3(1 - e^{-i\eta})(1 - e^{-i\theta}). \tag{66}$$

In the diagonal case we find that the amplification factor is maximized by taking $\xi = \eta = \theta = \pi$, which results in

$$T^{110}(\vec{\omega}_d) = \max\left(1, \left\lvert 1 - 6\omega_d + 12\omega_d^2 \right\rvert\right),$$

and hence the method is stable for $\omega_d \leq 1/2$ as indicated in Table III.

By also introducing double transverse propagation, as discussed in Section 2.3.1, we obtain Method $(1, 1, 1)$. It is possible to write T^{111} in the compact form

$$T^{111} = (1 - \omega_1(1 - e^{-i\xi}))(1 - \omega_2(1 - e^{-i\eta}))(1 - \omega_3(1 - e^{-i\theta})). \tag{67}$$

It can easily be shown that $T^{111}(\vec{\omega}) = 1$ for all $\vec{\omega}$ in the cube (62) and hence this method has optimal stability. (This is expected since Method $(1, 1, 1)$ is the shift and average scheme.)

Note that even though Method $(1, 1, 1)$ is only first-order accurate, it includes approximations to the third derivative term q_{xyz} coming from the double transverse propagation (and apparent from the product $\omega_1\omega_2\omega_3$ appearing in the expression for T^{111}). We will see for second-order methods that obtaining optimal stability requires including approximations to certain fourth-order derivatives (obtained by the double transverse propagation of correction waves in Method $(2, 2, 2)$).

4.2. Second-Order Methods

The simplest wave propagation method that is second-order accurate is Method $(2, 1, 0)$. Taking $m_1 = 2$ includes correction waves modeling the second derivative terms q_{xx}, q_{yy}, and q_{zz} in the Taylor expansion. Taking $m_2 = 1$ gives transverse propagation of the increment waves, which models the cross-derivative terms q_{xy}, q_{yz}, and q_{xz}. The amplification matrix is

$$T^{210} = T^{110} + \frac{1}{2}\omega_1(1 - \omega_1)(1 - e^{-i\xi})(1 - e^{i\xi}) + \frac{1}{2}\omega_2(1 - \omega_2)(1 - e^{-i\eta})(1 - e^{i\eta})$$

$$+ \frac{1}{2}\omega_3(1 - \omega_3)(1 - e^{-i\theta})(1 - e^{i\theta}). \tag{68}$$

In the diagonal case we find

$$T^{210}(\pi, \pi, \pi, \vec{\omega}_d) = 1 + 6\omega_d^2, \tag{69}$$

and hence this method is unstable for any ω_d. The method is stable in the special case where one of the velocities is zero, say $w = 0$ (and hence the corresponding directional Courant number is also zero, $\omega_3 = 0$). In this case the problem reduces to a two-dimensional problem and this method is optimally stable in two dimensions (this is what was called Method 3 in [27]). So Method $(2, 1, 0)$ is stable on faces of the cube (62), e.g., for all $\vec{\omega} = (\omega_1, \omega_2, 0)$ with $0 \leq \omega_1, \omega_2 \leq 1$, but nowhere in the interior as indicated in Table III and by the diagonal. Note that (69) gives the values in the table. This indicates that for this scheme the maximum is taken for wavenumbers equal to π.

In a fully three-dimensional problem our experience with first-order methods indicates that good stability requires including the corner-coupling terms q_{xyz}, and hence we must at least take $m_3 = 1$. The next simplest method includes transverse and double transverse propagation of the increment waves, along with correction waves in the normal direction, and is Method $(2, 1, 1)$. The expression for T^{211} is given by (68) with T^{110} replaced by T^{111}. Unfortunately this scheme is still unconditionally unstable for a fully three-dimensional problem, although the amplification factors are smaller than those for Method $(2, 1, 0)$. From the table also note that the scheme has an isolated point of stability at $\omega_d = 1.0$. For this value the scheme happens to be exact.

Transverse propagation of the correction wave must also be used to obtain a stable second-order-accurate method for fully three-dimensional problems. This means that $m_2 = 2$ and perhaps also $m_3 = 2$.

Method (2, 2, 0) has amplification factor

$$T^{220} = T^{210} + \frac{1}{2}\omega_1\omega_2(1 - \omega_1)(e^{i\xi} - 1)(1 - e^{-i\xi})(1 - e^{-i\eta})$$

$$+ \frac{1}{2}\omega_1\omega_3(1 - \omega_1)(e^{i\xi} - 1)(1 - e^{-i\xi})(1 - e^{-i\theta})$$

$$+ \frac{1}{2}\omega_1\omega_2(1 - \omega_2)(e^{i\eta} - 1)(1 - e^{-i\eta})(1 - e^{-i\xi})$$

$$+ \frac{1}{2}\omega_2\omega_3(1 - \omega_2)(e^{i\eta} - 1)(1 - e^{-i\eta})(1 - e^{-i\theta})$$

$$+ \frac{1}{2}\omega_1\omega_3(1 - \omega_3)(e^{i\theta} - 1)(1 - e^{-i\theta})(1 - e^{-i\xi})$$

$$+ \frac{1}{2}\omega_2\omega_3(1 - \omega_3)(e^{i\theta} - 1)(1 - e^{-i\theta})(1 - e^{-i\eta}). \tag{70}$$

According to Table III, this scheme is stable for $\omega_d \leq 0.5$, which is reasonable but still not optimal.

In Method (2, 2, 1), the increment wave propagates as in Method (1, 1, 1). The amplification factor is given by (70) but with T^{210} replaced by T^{211}. Like Method (2, 1, 0), T^{211} takes its maximum in the unstable regime for wavenumbers equal π. In this case T^{221} $(\pi, \pi, \pi, \vec{\omega}_d) = 1 - 18\omega_d^2 + 16_d\omega^3$ and the method is stable for $\omega_d \leq (1 + \sqrt{33})/16 \approx 0.4215$, in agreement with the table. Compared to Method (2, 2, 0), the stability region is slightly reduced, but the amplification factor outside the stable region is smaller and, as for Method (2, 1, 1), the scheme is exact for $\omega_d = 1.0$.

Finally, if the correction wave also propagates in a three-dimensional manner we obtain the full Method (2, 2, 2). The amplification factor for this method is

$$T^{222} = T^{221} - \frac{1}{2}\omega_1\omega_2\omega_3(1 - \omega_1)(e^{i\xi} - 1)(1 - e^{-i\xi})(1 - e^{-i\eta})(1 - e^{-i\theta})$$

$$- \frac{1}{2}\omega_1\omega_2\omega_3(1 - \omega_2)(e^{i\eta} - 1)(1 - e^{-i\eta})(1 - e^{-i\xi})(1 - e^{-i\theta})$$

$$- \frac{1}{2}\omega_1\omega_2\omega_3(1 - \omega_3)(e^{i\theta} - 1)(1 - e^{-i\theta})(1 - e^{-i\xi})(1 - e^{-i\eta}). \tag{71}$$

According to Table III, the wave propagation scheme is stable for $\omega_d \leq 1$, which is the best one can expect.

The results shown in Table III are for the scalar advection equation. We have also considered linear systems of equations such as acoustics and the linearized Euler equations with a nonzero background velocity. The stability limits depend on the particular system for methods such as the Lax–Wendroff and methods (1, 1, 0) and (2, 2, 0), but with roughly the same limits as seen for advection. Methods (1, 1, 1) and (2, 2, 2) remain stable for all Courant numbers up to 1 on the systems tested. A MATLAB script which computes these amplification factors may be found on the Web page [20].

4.3. Other Second-Order Discretizations

In this section we compare the stability results found for the wave propagation algorithms with that of the standard Lax–Wendroff method. We also consider what happens if the

centered approximations to second derivatives used in Lax–Wendroff, which forms the basis for the correction waves in our methods, are replaced by other standard approximations such as those used in the one-dimensional Beam–Warming or Fromm methods.

Consider a general method of the form

$$\bar{Q}_{IJK} = Q_{IJK} - \omega_1 \Delta_x Q_{IJK} - \omega_2 \Delta_y Q_{IJK} - \omega_3 \Delta_z Q_{IJK} + E_1 + E_2. \qquad (72)$$

The term E_1 includes the approximations of the pure second-order derivatives in the Taylor series, while E_2 models cross-derivative terms. Taking $E_1 = E_2 = 0$ gives the donor-cell upwind method, while the standard Lax–Wendroff method has

$$E_1^{LW} = -\frac{1}{2}\omega_1(1 - \omega_1)(\Delta_x Q_{I+1,JK} - \Delta_x Q_{IJK}) - \frac{1}{2}\omega_2(1 - \omega_2)(\Delta_y Q_{IJ+1,K} - \Delta_y Q_{IJK})$$

$$- \frac{1}{2}\omega_3(1 - \omega_3)(\Delta_z Q_{IJ,K+1} - \Delta_z Q_{IJK}). \qquad (73)$$

$$E_2^{LW} = \omega_1\omega_2\Delta_y^c\Delta_x^c Q_{IJK} + \omega_1\omega_3\Delta_z^c\Delta_x^c Q_{IJK} + \omega_2\omega_3\Delta_z^c\Delta_y^c Q_{IJK}, \qquad (74)$$

where $\Delta_x^c Q_{IJK}$ denotes the centered difference $(Q_{I+1,JK} - Q_{I-1,JK})/2$. The Lax–Wendroff amplification factor is

$$
\begin{aligned}
T^{LW} = {} & 1 - \frac{1}{2}\omega_1(e^{i\xi} - e^{-i\xi}) - \frac{1}{2}\omega_2(e^{i\eta} - e^{-i\eta}) - \frac{1}{2}\omega_3(e^{i\omega} - e^{-i\omega}) \\
& + \frac{1}{2}\omega_1^2(e^{i\xi} - 1)(1 - e^{-i\xi}) + \frac{1}{2}\omega_2^2(e^{i\eta} - 1)(1 - e^{-i\eta}) + \frac{1}{2}\omega_3^2(e^{i\omega} - 1)(1 - e^{-i\omega}) \\
& + \frac{1}{4}\omega_1\omega_2(e^{i\xi} - e^{-i\xi})(e^{i\eta} - e^{-i\eta}) + \frac{1}{4}\omega_1\omega_3(e^{i\xi} - e^{-i\xi})(e^{i\omega} - e^{-i\omega}) \\
& + \frac{1}{4}\omega_2\omega_3(e^{i\eta} - e^{-i\eta})(e^{i\omega} - e^{-i\omega}).
\end{aligned}
$$

Along the diagonal, Lax–Wendroff is stable for $\omega_d \le 0.1925$.

One might attempt to improve stability by replacing the centered approximations to cross-derivative terms by upwind approximations, using

$$E_2^{up} = \omega_1\omega_2\Delta_y\Delta_x Q_{ijk} + \omega_1\omega_3\Delta_z\Delta_x Q_{ijk} + \omega_2\omega_3\Delta_z\Delta_y Q_{ijk}$$

in place of E_2^{LW}. This gives Method (2, 1, 0) which was seen above to be unconditionally unstable. However, if we also replace E_1^{LW} by an upwind-biased approximation, stability can be restored. One possibility is to use the fully upwind Beam–Warming approximation introduced in [46] (see [25]):

$$E_1^{BW} = -\frac{1}{2}\omega_1(1 - \omega_1)(\Delta_x Q_{ijk} - \Delta_x Q_{i-1,jk}) - \frac{1}{2}\omega_2(1 - \omega_2)(\Delta_y Q_{ijk} - \Delta_y Q_{i,j-1,k})$$

$$- \frac{1}{2}\omega_3(1 - \omega_3)(\Delta_z Q_{ijk} - \Delta_z Q_{ij,k-1}).$$

Another is to use centered differences such as $\Delta_x^c Q_{IJK}$ in place of the upwind difference $\Delta_x Q_{IJK}$ in E_1^{LW}. This corresponds to Fromm's method [12] in one dimension, so we call

this

$$E_1^{Fr} = -\frac{1}{4}\omega_1(1-\omega_1)\big(\Delta_x^c Q_{ijk} - \Delta_x^c Q_{i-1,jk}\big) - \frac{1}{4}\omega_2(1-\omega_2)\big(\Delta_y^c Q_{ijk} - \Delta_y^c Q_{i,j-1,k}\big)$$
$$- \frac{1}{4}\omega_3(1-\omega_3)\big(\Delta_z^c Q_{ijk} - \Delta_z^c Q_{ij,k-1}\big).$$

Replacing E_1^{LW} by one of these and using E_2^{up} give methods we label Method BW(2, 1, 0) and Method Fr(2, 1, 0) for Beam–Warming and Fromm, respectively. One could then add in transverse propagation of the correction terms and perhaps double transverse propagation as well, giving methods such as BW(2, 2, 2). Only minor changes have to be made in the expressions for the amplification factors T^{210}, T^{211}, T^{220}, T^{221}, and T^{222}, in order to account for this change in the underlying approximation. For the BW-type approximation, the change is

$$\text{replace} \quad (e^{i\xi} - 1)(1 - e^{-i\xi}) \quad \text{by} \quad (e^{i\xi} - 1)(1 - e^{-i\xi})e^{-i\xi}.$$

Similar changes have to be made for corresponding terms involving η and θ. Likewise, the changes to be made for the inclusion of Fromm-type discretization are

$$\text{replace} \quad (e^{i\xi} - 1)(1 - e^{-i\xi}) \quad \text{by} \quad \frac{1}{2}(1 - e^{-i\xi})(e^{i\xi} - e^{-i\xi}).$$

These modified methods are interesting to study since the effect of adding certain limiters is to give an upwind bias toward one of these methods. The full effect of adding a limiter is more complicated since the methods are then nonlinear and von Neumann analysis does not apply. Nonetheless, it may be reassuring to know that we are switching to a method that is also stable in its own right.

Table IV gives a summary of stability results along the diagonal for these modified methods. One significant result is that none of these methods is unconditionally unstable in the manner of Method LW(2, 1, 0) or LW(2, 1, 1). In general, the Fromm methods have the

TABLE IV
The Amplification Factor $\mathcal{T}(\vec{\omega}_d)$ versus the CFL Number $\omega_d = \omega_1 = \omega_2 = \omega_3$ for the Scalar Problem

ω_d	$\max_{\xi,\eta,\theta}|T|$, Beam–Warming					$\max_{\xi,\eta,\theta}|T|$, Fromm				
	T^{210}	T^{211}	T^{220}	T^{221}	T^{222}	T^{210}	T^{211}	T^{220}	T^{221}	T^{222}
0.1	1.00	1.00	1.00	1.00	1.00	1.00	1.00	1.00	1.00	1.00
0.2	1.00	1.00	1.00	1.00	1.00	1.00	1.00	1.00	1.00	1.00
0.3	1.00	1.20	1.00	1.00	1.00	1.00	1.00	1.00	1.00	1.00
0.4	1.00	1.43	1.38	1.00	1.00	1.00	1.00	1.00	1.00	1.00
0.5	1.00	1.50	2.50	1.50	1.00	1.00	1.00	1.00	1.00	1.00
0.6	1.00	1.45	3.74	2.01	1.00	1.72	1.00	1.72	1.01	1.00
0.7	1.42	1.32	4.95	2.20	1.00	2.68	1.00	2.68	1.03	1.00
0.8	2.92	1.18	5.99	1.90	1.00	3.88	1.00	3.88	1.02	1.00
0.9	4.78	1.05	6.72	1.19	1.00	5.32	1.00	5.32	1.02	1.00
1.0	7.00	1.00	7.00	1.00	1.00	7.00	1.00	7.00	1.00	1.00
1.01	7.24	1.08	7.00	1.25	1.00	7.18	1.06	7.18	1.11	1.06

largest stability regions, though in the case of Method (2, 2, 2), all three approaches give optimally stable methods.

4.4. Limiter Influence and Wavenumber Dependency

The numerical example in Section 3.2 was also studied in [19]. The method used was (2, 1, 1) at a Courant number of about 0.9, and the computation did not suffer from any instability problems. From other numerical experiments we have observed that the uncon- ditionally unstable methods (2, 1, 0) and (2, 1, 1) do not behave as badly as the discussion above may indicate. This is especially true for Method (2, 1, 1). But even Method (2, 1, 0) may produce nice results when applied to nonlinear problems *if* limiters are used. This indicates that the instability is strongest for large wavenumbers. Limiters are assumed to be most effective in this range. In this section we reconsider the two test problems from the previous section and examine how the amplification factor depends on wavenumbers and to some extent on limiters.

To simplify the discussion, we consider the case of equal wavenumbers, i.e., $\xi = \eta = \theta$. In Fig. 10, the absolute value of the amplification factor versus the wavenumber for the scalar problem is depicted for three different values of the Courant number ω_d. The analytical expressions derived in the previous section are used. For all schemes, $|T|$ is symmetric about $\xi = 0$, and in the figures only $0 \leq \xi \leq \pi$ is given.

As expected, the stable methods (1, 1, 1) and (2, 2, 2) are uniformly bounded by one, and the former scheme is more dissipative than the latter. When it comes to the unstable schemes, Method (2, 1, 0) is more unstable than Method (2, 1, 1) for nearly all wavenumbers and Courant numbers.

These results may be utilized to find initial conditions that trigger instabilities in the schemes. Consider the initial condition

$$q_0(x, \ y, \ z) = \sin(2\pi nx + 2\pi ny + 2\pi nz), \tag{75}$$

where n is a positive integer. Assume that the computational domain is $[0, 1] \times [0, 1] \times [0, 1]$, that $\Delta x = \Delta y = \Delta z$, and that periodic boundary conditions are used on all boundaries. The wavelength in the Fourier mode (63) is $2\pi \Delta x/\xi$, and in (75) the wavelength is $1/n$. Hence,

$$\xi = \frac{2\pi n}{N},$$

where N is the number of cells in each coordinate direction. Since the shortest wavelength obtainable on the grid is $2\Delta x$, acceptable values for n are $1, 2, \ldots, N/2$, assuming that N is even.

An estimate for the amplification factor is obtain by considering the ratio

$$\max_{IJK}|\bar{Q}_{IJK}|/\max_{IJK}|\bar{Q}_{IJK}|. \tag{76}$$

An average value of this ratio for a number of steps is used. Due to roundoff errors, a com- putation may trigger instabilities, even though the wavenumbers used should give stability. In such cases, the average is estimated based on "stable steps."

In plots on the right side of Fig. 10, the estimated amplification factor is depicted with "○" symbols for Method (2, 1, 1). In these computations $N = 40$ and $n = 5, 10, 15, 20$ are used. The symbols lie very close to the curves as expected.
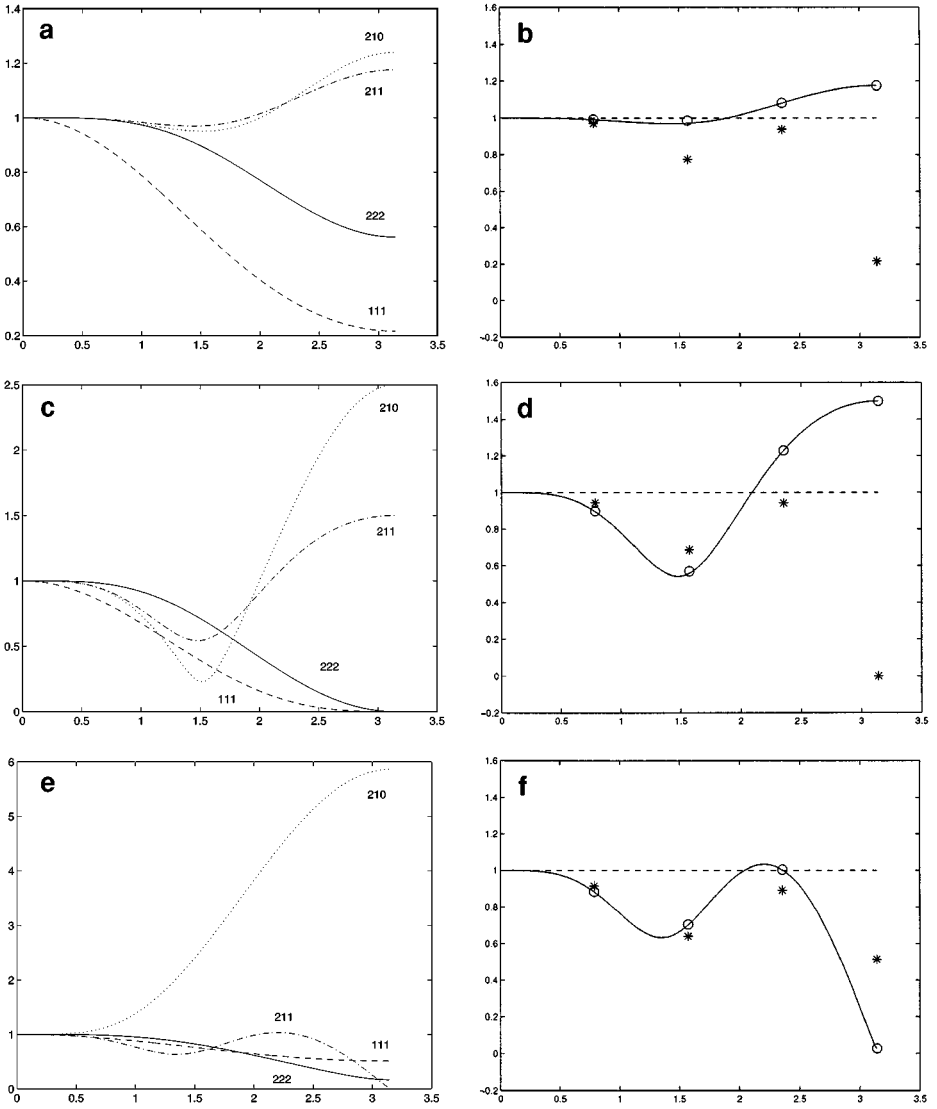
FIG. 10. The absolute value of the amplification factor versus the wavenumber $\xi = \eta = \theta$ for the scalar advection problem. The Courant numbers are: (top row) $\omega_d = 0.2$, (middle row) $\omega_d = 0.5$, (bottom row) $\omega_d = 0.9$. Plots in the left column show results for four different methods, 111, 210, 211, and 222. The right column shows the effect of limiters for the case of Method $(2, 1, 1)$ (on a different scale). The circles $(\bigcirc)$ correspond to numerical experiments, while the $\times$-marks show the same numerical experiments when the MC limiter is incorporated.

It is now possible to study the effect of limiters on stability. The computations are redone, but now with the MC limiter turned on. The estimates for the ratio (76) are marked using $\times$-marks. The overall picture is that the limiters may prevent the solution from going unstable for all Courant numbers. Note that when $n = 20$, yielding a wavelength of $2\Delta x$, the gradient in the numerical solution changes sign from one cell to the other. In this case the limiter becomes zero, the high-order terms are switched off and the scheme is equivalent to Method $(1, 1, 1)$.

Limiters are constructed to reduce oscillations near discontinuities. They are not intended to increase the stability range of the scheme. Nevertheless, it seems that the use of limiters has a positive effect on Method (2, 1, 1). Computations similar to those reported above show that this also is the case to some extent for Method (2, 1, 0). Note, however, that there is no reason to use Method (2, 1, 1), since it involves nearly the same amount of work as the stable Method (2, 2, 2). Method (2, 1, 0) should probably not be trusted in general, even though it produces good looking results on certain problems.

5. CONCLUSIONS

In this paper, a class of three-dimensional wave propagation methods for conservation laws is constructed. By using proper wave propagation, a method which is stable for Courant number up to 1 is obtained. Simpler versions of the method appear to be stable in practice due to the effects of the nonlinear limiter function even though the unlimited versions are unstable for linear problems. This is analyzed in Section 4. In practice, we recommend Method (2, 2, 2) as the most robust and stable of the second-order multidimensional methods.

This three-dimensional scheme generalizes the two-dimensional approach for systems in [28] and the 3D scheme for scalar advection in [27]. The wave propagation method is implemented in Fortran, and is included in the software package CLAWPACK, freely available on the Web.

The methods have been applied to the Euler equations as a sample application. Though the examples used in this paper are written in conservative form, the methods, as implemented in CLAWPACK, handle the more general class of hyperbolic equations (3) as discussed in [28].

To efficiently solve realistic problems in three space dimensions, adaptive mesh refinement is often a necessity. The algorithms described here are being implemented in the BEARCLAW package (Boundary Embedded Adaptive Refinement) being developed by Sorin Mitran at the University of Washington. This follows the AMRCLAW adaptive mesh refinement procedures developed with Marsha Berger, as described in two space dimensions in [4], but is a tree-based Fortran-90 package which will ultimately be augmented by boundary-embedded Cartesian grid techniques for handling general geometries. For large three-dimensional problems it may also be necessary to use parallel processing, and MPI directives are easily incorporated in the BEARCLAW code. Another software package based on these algorithms is ZPLCLAW, being developed by Turkiyyah and Wu [47] using the ZPL parallel programming language of Snyder [40]. Pointers to these other packages may be found on the CLAWPACK, webpage [29]. Supplementary material for this paper and animations of some of the results presented may be found at [20].

REFERENCES

1. T. J. Barth, On unstructured grids and solvers, in *Von Karman Institute for Fluid Dynamics Lecture Series*, 90-03 (1990).

2. J. B. Bell, C. N. Dawson, and G. R. Shubin, An unsplit, higher order Godunov method for scalar conservation laws in multiple dimensions, *J. Comput. Phys.* **74**, 1 (1988).

3. M. J. Berger and R. J. LeVeque, AMRCLAW software. Available at http://www.amath.washington.edu/~rjl/amrclaw/.

4. M. J. Berger and R. J. LeVeque, Adaptive mesh refinement using wave-propagation algorithms for hyperbolic systems, *SIAM J. Numer. Anal.* **35**, 2298 (1998).

5. S. J. Billett, *A Class of Upwind Methods for Conservation Laws*, Ph.D. thesis (Cranfield University, 1994).

6. J. P. Boris and D. L. Book, Flux corrected transport I, SHASTA, a fluid transport algorithm that works, *J. Comput. Phys.* **11**, 38 (1973).

7. P. Colella, Multidimensional upwind schemes for hyperbolic conservation laws, *J. Comput. Phys.* **87**, 171 (1990).

8. P. Colella and P. Woodward, The piecewise–parabolic method (PPM) for gas-dynamical simulations, *J. Comput. Phys.* **54**, 174 (1984).

9. M. Crandall and A. Majda, The method of fractional steps for conservation laws, *Numer. Math.* **34**, 285 (1980).

10. Wai Sun Don and C. B. Quillen, Numerical simulation of shock-cylinder interactions: I. Resolution, *J. Comput. Phys.* **122**, 244 (1995).

11. T. Fogarty and R. J. LeVeque, High-resolution finite volume methods for acoustics in a rapidly-varying heterogeneous medium, in *Proc. Fourth Int. Conf. on Wave Propagation* (Golden, CO, SIAM, 1998) (ftp://amath.washington.edu/pub/rjl/papers/tf-rjl:wave98.ps.Z).

12. J. E. Fromm, A method for reducing dispersion in convective difference schemes, *J. Comput. Phys.* **3**, 176 (1968).

13. T. Fogarty and R. J. LeVeque, High-resolution finite volume methods for acoustics in periodic or random media, *J. Acoust. Soc. Am.* **106**, 17 (1999).

14. E. Godlewski and P.-A. Raviart, *Numerical Approximation of Hyperbolic Systems of Conservation Laws* (Springer–Verlag, New York, 1996).

15. S. K. Godunov, Finite difference methods for numerical computations of discontinuous solutions of equations of fluid dynamics, *Mat. Sb.* **47**, 271 (1959).

16. J. J. Gottlieb and P. T. Groth, Assessment of Riemann solvers for unsteady one-dimensional inviscid flows of perfect gases, *J. Comput. Phys.* **78**, 437 (1988).

17. A. Harten and J. M. Hyman, Self-adjusting grid methods for one-dimensional hyperbolic conservation laws, *J. Comput. Phys.* **50**, 235 (1983).

18. D. Kröner, *Numerical Schemes for Conservation Laws* (Wiley–Teubner, 1997).

19. J. O. Langseth and R. J. LeVeque, Three-dimensional Euler computations using CLAWPACK, in *Conf. on Numer. Meth. for Euler and Navier–Stokes Eq.*, edited by P. Arminjon (Navier–Stokes, Montreal, 1995), available at ftp://amath.washington.edu/pub/rjl/papers/jol-rjl:montreal95.ps.Z (1995).

20. J. O. Langseth and R. J. LeVeque, Web page containing supplementary material for this paper. Available at http://www.amath.washington.edu/~rjl/clawpack/3dpaper.html.

21. J. O. Langseth, *Wave Propagation Methods, Operator Splitting, and Front Tracking for Hyperbolic Problems*, Ph.D. thesis, (University of Oslo, 1996).

22. P. D. Lax, Hyperbolic systems of conservation laws, II, *Comm. Pure Appl. Math.* **10**, 537 (1957).

23. P. D. Lax and B. Wendroff, Difference schemes for hyperbolic equations with high order of accuracy, *Comm. Pure Appl. Math.* **18**, 381 (1964).

24. B. P. Leonard, M. K. MacVean, and A. P. Lock, Positivity-preserving numerical schemes for multidimensional advection, NASA Technical Memorandum 106055, ICOMP-93-05, (1993).

25. R. J. LeVeque, *Numerical Methods for Conservation Laws* (Birkhäuser–Verlag, 1990).

26. R. J. LeVeque, Simplified multi-dimensional flux limiter methods, in *Numerical Methods for Fluid Dynamics* 4, edited by M. J. Baines and K. W. Morton (Oxford Univ. Press, 1993), p. 175.

27. R. J. LeVeque, High-resolution conservative algorithms for advection in incompressible flow, *SIAM J. Numer. Anal.* **33**, 627 (1996).

28. R. J. LeVeque, Wave propagation algorithms for multi-dimensional hyperbolic systems, *J. Comput. Phys.* **131**, 327 (1997).

29. R. J. LeVeque, CLAWPACK software, available on the Web at http://amath.washington.edu/~claw.

30. J. J. Quirk and S. Karni, *On the Dynamics of a Shock–Bubble Interaction, J. Fluid Mech.* **318**, 129 (1996).

31. Y. B. Radvogin, *Quasi-monotonous Multidimensional Differential Schemes with Second Order Accuracy* (Soviet Academy of Science Preprint, 1991).

32. R. D. Richtmyer and K. W. Morton, *Difference Methods for Initial-Value Problems* (Wiley–Interscience, 1967).

33. P. L. Roe, Approximate Riemann solvers, parameter vectors, and difference schemes, *J. Comput. Phys.* **43**, 357 (1981).

34. P. L. Roe and D. Sidilkover, Optimum positive linear schemes for advection in two and three dimensions, *J. Numer. Anal.* **29**, 1542 (1992).

35. P. L. Roe, Sonic flux formulae, *SIAM J. Sci. Stat. Comput.* **13**, 611 (1992).

36. J. Saltzman, *Monotonic Difference Schemes for the Linear Advection Equation in Two and Three Dimensions*, Los Alamos Report LA-UR-87-2479 (1987).

37. J. Saltzman, An unsplit 3-D upwind method for hyperbolic conservation laws, *J. Comput. Phys.* **115**, 153 (1994).

38. P. K. Smolarkiewicz and W. W. Grabowski, The multidimensional positive definite advection transport algorithm: Nonoscillatory option, *J. Comput. Phys.* **86**, 355 (1990).

39. J. Smoller, *Shock Waves and Reaction-diffusion Equations* (Springer–Verlag, New York, 1983).

40. L. Snyder, *A Programmer's Guide to ZPL* (MIT Press, 1999).

41. G. Strang, On the construction and comparison of difference schemes, *SIAM J. Num. Anal.* **5**, 506 (1968).

42. J. C. Strikwerda, *Finite Difference Schemes and Partial Differential Equations* (Wadsworth, 1989).

43. P. K. Sweby, High resolution schemes using flux limiters for hyperbolic conservation laws, *SIAM J. Num. Anal.* **21**, 995 (1984).

44. E. F. Toro, *Riemann Solvers and Numerical Methods for Fluid Dynamics: A Practical Introduction* (Springer–Verlag, Berlin, 1997).

45. J. Trangenstein, *An Unsplit Godunov Method for Three-Dimensional Polymer Flooding*, preprint (1993).

46. R. F. Warming and R. M. Beam, Upwind second-order difference schemes and applications in unsteady aerodynamic flows, in *Proc. AIAA 2nd Computational Fluid dynamics* Conference (Hartford, CN, 1975).

47. H. Wu, G. Turkiyyah, and W. Keirouz, ZPLCLAW: A parallel portable toolkit for wave propagation problems, *Proc. ASCE Structures 2000 Congress* (Philadelphia, PA, 2000).

48. B. van Leer, Towards the ultimate conservative difference scheme. IV. A new approach to numerical convection, *J. Comput. Phys.* **23**, 276 (1977).

49. B. van Leer, Towards the ultimate conservative difference scheme. V. A second order sequel to Godunov's method, *J. Comput. Phys.* **32**, 101 (1979).

50. S. T. Zalesak, Fully multidimensional flux corrected transport algorithms for fluids, *J. Comput. Phys.* **31**, 335 (1979).

51. Viz software, Available on the Web at `ftp://ftp.ffi.no/spub/stsk/viz/index.html`.